The N-terminus of Stag1 is required to repress the 2C program by maintaining rRNA expression and nucleolar integrity.

Dubravka Pezic[1], Samuel Weeks[1], Wazeer Varsally[1], Pooran S. Dewari[2], Steven Pollard[2], Miguel R. Branco[3], Suzana Hadjur[1]*

1 Research Department of Cancer Biology, Cancer Institute, University College London, 72 Huntley Street, London, United Kingdom

2 MRC Centre for Regenerative Medicine, University of Edinburgh, Edinburgh, United Kingdom

3 Blizard Institute, Barts and The London School of Medicine and Dentistry, QMUL, London, United Kingdom

* Correspondence: s.hadjur@ucl.ac.uk

ABSTRACT

Several studies have shown a role for Stag proteins in cell identity. Our understanding of how Stag proteins contribute to cell identity have largely been focused on its roles in chromosome topology as part of the cohesin complex and the impact on protein-coding gene expression. Furthermore, several Stag paralogs exist in mammalian cells with non-reciprocal chromosome structure and cohesion functions. Why cells have so many Stag proteins and what specific functions each Stag protein performs to support a given cell state are poorly understood. Here we reveal that Stag1 is the dominant paralog in mouse embryonic stem cells (mESC) and is required for pluripotency. Through the discovery of diverse, naturally occurring Stag1 isoforms in mESCs, we shed new light not only on the unique ends of Stag1 but also the critical role that their levels play in stem cell identity. Furthermore, we revel a new role for Stag1, and specifically its unique N-terminal end, in regulating nucleolar integrity and safeguarding mESCs from totipotency. Stag1 is localised to repressive perinucleolar regions, bound at repeats and interacts with Nucleolin and TRIM28. Loss of the Stag1 N-terminus, leads to decreased LINE-1 and rRNA expression and disruption of nucleolar structure and function which consequently leads to activation of the two-cell-like (2C-LC)-specific transcription factor DUX and conversion of pluripotent mESCs to totipotent 2C-LCs. Our results move beyond protein-coding gene regulation via chromatin loops into a new role for Stag1 in repeat regulation and nucleolar structure, and offer fresh perspectives on how Stag proteins contribute to cell identity and disease.

INTRODUCTION

Cohesin is a ubiquitously expressed, multi-subunit protein complex that has fundamental roles in cell biology including sister chromosome cohesion, 3D chromatin topology and regulation of cell identity [1-6]. Much of our understanding of how cohesin contributes to cell identity has been studied in the context of its roles in protein-coding gene expression and 3D organization of interphase chromatin structure [7-15]. Indeed, loss of cohesin and its regulators results in a dramatic loss of chromatin topology at the level of Topologically Associated Domains (TAD) and chromatin loops, albeit with modest changes to gene expression [16-22]. This suggests that cohesin's roles in development and disease extend beyond gene expression regulation and highlight the need to re-evaluate how cohesin regulators shape the structure and function of the genome.

The association of cohesin with chromosomes is tightly controlled by several regulators, including the Stromalin Antigen protein (known as Stag or SA), which has been implicated in cell identity regulation and disease development [2,3,23-26]. Stag proteins interact with the Rad21 subunit of cohesin and mediate its association with DNA and CTCF [27-30]. Mammalian cells express multiple Stag paralogs, which have >90% sequence conservation in their central domain yet perform distinct functions [31-34]. It is likely that the divergent N- and C-terminal regions provide functional specificity. For example, the N-terminus of Stag1 contains a unique AT-hook [35] which is required for its preferential participation in telomere cohesion [31]. However, the underlying mechanisms by which Stag proteins and their divergent ends influence cell identity are largely unknown.

The nucleolus is a multifunctional nuclear compartment which coordinates ribosome biogenesis with cell cycle control and mRNA processing [36]. It forms through self-organization of its constituent proteins and the rDNA gene clusters into a tripartite, phase separated condensate [37,38] which is intimately connected to overall nuclear organization [39]. In line with its liquid-like properties, the nucleolus is itself plastic, undergoing dramatic changes in response to cell cycle, metabolic or developmental

51 cues. For example, functional nucleoli play an important role in the control of cell identity
52 during early mouse development [40]. Two-cell (2C) stage totipotent embryos exhibit
53 'immature' nucleoli with poorly defined structure and low levels of perinucleolar
54 heterochromatin [41,42]. This global chromatin accessibility contributes to the expression
55 of the 2C-specific transcription factor DUX and the subsequent activation of MERVL
56 elements [43,44]. As the embryo reaches the 8-cell stage, cells harbour fully mature
57 phase-separated nucleoli, defined heterochromatin around the nucleolar periphery [45]
58 and robust rRNA expression, all of which are essential for cells to commit to
59 differentiation [40,46]. In contrast, mouse embryonic stem cells (mESC) exhibiting
60 nucleolar stress lead to conversion to 2C-like cell (2C-LC) identity *in vitro* [47] and
61 nucleolar proteins that control rRNA transcription and processing are essential for 2C-
62 LC repression [48]), highlighting the tight relationship between rRNA levels, nucleolar
63 structure and cell identity.

64 It is known that cohesin is necessary for nucleolar integrity in yeast. Core cohesin
65 subunits have been shown to bind to the non-transcribed region of the rDNA locus [49]
66 and the 35S and 5S genes form loops that are dependent on Eco1, the cohesin subunit
67 known to acetylate Smc3 and thus stabilize cohesin rings on chromatin [50].
68 Consequently, yeast with eco1 mutations exhibit disorganised nucleolar structure and
69 defective ribosome biogenesis.

70 Here we reveal a novel role for Stag1, and in particular its unique N-terminal end,
71 in regulating nucleolar integrity and 2C repression to maintain mESC cell identity.
72 Stag1 binds to repeats associated with nucleolar structure and function including rDNA
73 and LINE-1 and interacts with the Nucleolin/TRIM28 complex that resides within
74 perinucleolar chromatin to maintain nucleolar integrity. Loss of Stag1 or specifically the
75 N-terminus in mESCs leads to reduced nascent rRNA and LINE-1, nucleolar disruption,
76 increased expression of DUX and conversion of mESCs to totipotent 2C-LC cells. In
77 addition to presenting a new role for Stag1 in repeat regulation, nucleolar structure and
78 translation control, our results also reveal a previously unappreciated transcriptional
79 diversity of Stag1 in stem cells and highlights the complexity of cohesin regulation in

80 mammalian cells. We show that cells change both the levels of Stag paralogs as well
81 as the balance of isoforms to control cell identity and point to the importance of the
82 divergent, unstructured ends of Stag1 proteins in nuclear body structure and cell fate
83 control. Our results offer fresh perspectives on how Stag proteins, known to be pan-
84 cancer targets [3] contribute to cell identity and disease.

85

86 **RESULTS**

87 **A functional change in cohesin regulation in cells of different potential.**
88 We analysed the expression levels of cohesin regulators in mESCs by qRT-PCR at
89 different stages of pluripotency. During the transition between naïve (2i mESC) and
90 primed epiblast-like (EpiLC) pluripotent cells *in vitro*, levels of the core cohesin subunits
91 Smc1 and Smc3 do not change, while Stag1 becomes downregulated and Stag2
92 becomes upregulated (Fig. 1a, b, S1a, b). This is supported by western blot (WB)
93 analysis where we observe a 2-3-fold higher level of chromatin-associated Stag1
94 compared to Stag2 protein in naïve (2i) mESC, while Stag2 levels are 5-10-fold higher
95 in EpiLC (Fig. 1b, S1c). These results, together with similar observations [26], identify
96 Stag1 as the dominant paralog in naïve mESC and suggest that a switch between
97 Stag1 and Stag2 may represent a functionally important change in cohesin regulation at
98 different stages of pluripotency.

99

100 **Stag1 is required for pluripotency.**
101 To investigate the functional importance of Stag1 in the regulation of pluripotency, we
102 first established a Stag1 knockdown (KD, 'siSA1', Methods) strategy using siRNAs. This
103 resulted in a significant reduction of Stag1 at the mRNA and protein levels (4-5-, 8-10-
104 fold, respectively), in both serum-grown (FCS) and naive mESC without affecting the
105 cell cycle (Fig. 1c, S1d-f). Using Nanog as a marker of naïve pluripotency, we observed
106 a significant downregulation of Nanog mRNA and protein levels within 24hrs of Stag1
107 KD in mESC (Fig. 1d, S1g), suggesting that Stag1 may be required for pluripotency.

108 Global analysis of the mESC transcriptome using RNA-sequencing upon siRNA-
109 mediated Stag1 KD revealed that 375 genes were up- and 205 genes were down-
110 regulated by at least 2-fold (Fig. 1e). Among the downregulated group were genes
111 known to have roles in the maintenance of pluripotency (ie. Nanog, Tbx3, Esrrb, Klf4),
112 while genes associated with exit from pluripotency (Dnmt3b, Fgf5) and differentiation
113 (ie. Pou3f1 (Oct6), Sox11) were upregulated (Fig. 1e). Gene Set Enrichment Analysis
114 (GSEA) [51,52] confirmed a reproducible loss of naïve pluripotency-associated gene
115 signature and enrichment for genes associated with primed pluripotency upon Stag1 KD
116 (Fig. 1f, S1h).

117 The loss of the naïve transcriptional programme upon Stag1 KD suggests that
118 mESCs may require Stag1 for the maintenance of self-renewal. To test this, we plated
119 cells in self-renewal conditions at clonal density and determined the proportion of
120 undifferentiated cells upon Stag1 KD by measuring the area occupied by the colonies
121 with high alkaline phosphatase activity (AP+). In scrambled siRNA-treated controls, 52%
122 of plated cells retain their naïve state, identified by AP+ colonies which was not
123 significantly different from untreated cells. Upon Stag1 KD, both the proportion of AP+
124 colonies and the area they occupy decreased by an average of 20% compared to
125 siRNA controls, indicating that mESCs have a reduced ability to self-renewal in the
126 absence of Stag1 (Fig. 1g, S5d).

127 We validated these observations by using CRISPR/Cas9 to knock-in an
128 mNeonGreen-FKBP12^{F36V} tag [53] at the C-terminus of both alleles of the endogenous
129 Stag1 locus (SA1^{NG_FKBP}) in mESC (Fig. 1h, S1i-k). Upon dTAG addition, Stag1 protein
130 is robustly degraded in a SA1^{NG_FKBP} mESC clone (Fig. 1h, S1k). As we had previously
131 observed with siRNA treatment, dTAG-mediated degradation of Stag1 led to a reduction
132 in Nanog protein (reduced by 24% compared to DMSO controls) (Fig. 1h) and self-
133 renewal potential was reduced by an average of 38% compared to DMSO-treated cells
134 (Fig. 1i). Together, our results are consistent with a requirement for Stag1 in the control
135 of naïve pluripotency.

136 **STAG1 localizes to both euchromatin and heterochromatin.**

137 To understand how Stag1 contributes to pluripotency, we first investigated its
138 subcellular localization. Live-cell imaging of Hoechst-labelled SA1^{NG_FKBP} mESC
139 revealed the expected and predominant localisation of Stag1 in the nucleus with a
140 notable punctate pattern within the nucleoplasm (Fig. 2a). Stag1 was also colocalised
141 with Hoechst-dense regions (Fig. 2a, arrows) and enriched in Hoechst-dense foci
142 compared to the whole nucleus (Fig. 2b). This was of interest since Hoechst stains AT-
143 rich heterochromatin which is enriched around the nucleolus, at the nuclear periphery
144 and in discreet foci within the nucleoplasm [39,54]. Acute degradation of Stag1 in
145 SA1^{NG_FKBP} mESCs resulted in increased Hoechst signal intensity (Fig. 2c) and a
146 significant increase in Hoechst foci volume (Fig. 2d). siRNA-mediated Stag1 KD mESCs
147 revealed similar changes to heterochromatin, as assessed by DAPI and H3K9me3
148 staining (Fig. S2a, b).
149 These observations prompted us to re-analyse STAG1 chromatin
150 immunoprecipitation followed by sequencing (ChIP-seq) data in mESC [26,55]. We
151 calculated the proportion of STAG1 peaks that overlapped genes, repeats (within the
152 Repeat Masker annotation), introns and intergenic regions not already represented (see
153 Methods). Of the 18,600 STAG1 peaks identified, the majority (76%) are bound to
154 genomic sites that are distinct from protein-coding genes including at repetitive
155 elements and intergenic regions (Fig. S2c). Indeed, STAG1 binding was enriched at
156 specific repeat families above random expectation (Fig. 2e). These included the DNA
157 transposon and Retrotransposon classes, both known to form constitutive
158 heterochromatin in differentiated cell types, are expressed in early development and
159 involved in regulation of cell fate [56,57]. Specifically, STAG1 was enriched at SINE B3
160 and B2-Mm2 elements (previously shown to be enriched at TAD borders [58]); several
161 LTR families, two of which have been previously shown to be associated with CTCF
162 (LTR41, LTR55) [59] and at evolutionary young and active families of LINE1 elements
163 (L1Tf, L1A) (Fig. 2e, f, S2e). We also found that several SINE B3 elements located
164 within the intergenic spacer (IGS) of the consensus rDNA locus were bound by STAG1
165 (Fig. 2g). The binding of STAG1 at repeats may be dependent on CTCF since many of
166 the bound repeats contained CTCF motifs (Fig. S2d).

167 RNA-seq of siSA1-treated mESC did not reveal dramatic changes in steady-state
168 transcription of repetitive elements. However, qRT-PCR analysis using primers to ORF1
169 of Stag1-bound LINE1 and pre-rRNA revealed reduced expression compared to
170 controls (Fig. S2f), suggesting a possible role for Stag1 in the control of repeat
171 expression. Together with the microscopy results, the profile of STAG1 peaks suggests
172 that the role of Stag1 in mESCs may extend beyond protein-coding gene regulation.
173
174 **STAG1 supports nucleolar structure.**
175 In mESCs, LINE1 transcripts have been shown to act as a nuclear RNA scaffold for the
176 interaction with the nucleolar protein Nucleolin (NCL), a regulator of rRNA transcription,
177 and the co-repressor TRIM28 (Kap1) [60]. The complex promotes rRNA synthesis,
178 nucleolar structure and self-renewal in mESC [56]. Since depletion of Stag1 results in a
179 loss of self-renewal and reduced rRNA expression and Stag1 was enriched at LINE1
180 and rDNA, we considered whether Stag1 was supporting pluripotency through nucleolar
181 structure and function. We were not able to use spinning disk microscopy to assess the
182 co-localization of Stag1 with nucleolar proteins in live cells. Instead, we used confocal
183 imaging of $SA1^{NG_FKBP}$ mESC stained with NCL. We observed a similar amount of SA1-
184 NeonGreen ($SA1^{NG}$) within the nucleolus compared to the nucleus of mESC (Fig. 2h, i).
185 Notably, upon dTAG-treatment of $SA1^{NG_FKBP}$ mESC, there was a significant increase in
186 NCL signal intensity (Fig. 2j) as well as increased numbers of nucleolar foci in both
187 dTAG-treated $SA1^{NG_FKBP}$ and in siSA1 KD mESCs (Fig. 2k, S2g, h), reminiscent of
188 changes observed during mESC differentiation [61]. Further, STAG1 immunoprecipitation
189 followed by WB in mESC revealed an interaction with both NCL and Trim28 (Fig. 2l),
190 suggesting a direct effect of Stag1 on nucleolar structure and rRNA expression.
191
192 **Stag1 expression is highly regulated in mESCs.**
193 We consistently observed several immunoreactive bands on Stag1 WB (Fig. 2l, arrows),
194 which were enriched in mESC (Fig. 1b). In order to gain a full perspective on how Stag1
195 may be contributing to nucleolar structure and pluripotency, we first investigated
196 whether *STAG1* may be regulated at the level of transcription in mESCs. Several lines

197 of evidence suggested that this may be the case. First, STAG1 levels are higher in 2i-
198 grown compared to FCS-grown mESCs, a culture condition that supports a mix of naïve
199 and primed cells (Fig. S1b, d) and second, primers positioned along the length of
200 STAG1 amplify mRNAs that respond differently to differentiation (Fig. 1a). Thus, we
201 employed a series of approaches to comprehensively characterize Stag1 mRNAs. First,
202 we used RACE (Rapid Amplification of cDNA Ends) to characterize the starts and ends
203 of Stag1 mRNAs directly from mESCs. 5' RACE uncovered four novel alternative
204 transcription start sites (TSS) in mESCs; ~50kb upstream of the canonical Stag1 TSS
205 (referred to as 'SATS', and previously identified in [62]) (Fig. 3a, d, S3a); between
206 canonical exon 1 and exon 2 (referred to as alternative exon 1 or altex1) (Fig. 3a, d,
207 S3d); and at exons 6 and 7 (Fig. 3a, d, S3a). Interestingly, the TSS located at exon 7
208 (e7) was preceded by a sequence located *in trans* to the STAG1 gene, carrying simple
209 repeats and transcription factor binding sites (Fig. 3b). While the frequency of this
210 alternative TSS was significantly lower than the other TSSs, it was identified in multiple
211 RACE replicates, indicating that it may be present in a subset of the mESC population.
212 We also discovered widespread alternative splicing in the 5' region of Stag1, with
213 particularly frequent skipping of exons 2 and 3 (e2/3Δ) and exon 5 (e5Δ) (Fig. 3d, S3a,
214 f). Using 3' RACE, we detected an early termination site in intron 25 and inclusion of an
215 alternative exon 22 introducing an early STOP codon, as well as several 3'UTRs (Fig. 3
216 c, d, S3c).
217 Next, PCR- and Sanger sequencing-based clonal screening confirmed that the
218 newly discovered 5' and 3' ends represent true Stag1 transcript ends, validated the
219 existence of the e2/3Δ and e5Δ isoforms, confirmed their enrichment in naïve mESCs
220 compared to differentiated mouse embryonic fibroblasts (MEFs) and uncovered an
221 isoform lacking exon 31 which encodes a basic domain embedded in the otherwise
222 acidic C-terminal region of Stag1 (e31Δ) (Fig. S3d). To determine the complete
223 sequences of the Stag1 transcript isoforms and to use a non-PCR-based approach, we
224 performed long-read PacBio Iso-seq from 2i mESC RNA (Fig. 3e). This confirmed the
225 diversity of the Stag1 5' and 3'UTRs, the e31Δ isoform, multiple TSSs including SATS,
226 and early termination events, including in i22 and i25 (Fig. 3e, S3e). Importantly, these

227 transcripts all had polyA tails, in support of their protein-coding potential. Finally, we
228 validated and quantified the newly discovered splicing events by calculating the
229 frequency (percentage spliced in (PSI)) of exon splicing in our RNA-seq as well as in
230 published data using the VAST-tools method [63]. This confirmed the presence of Stag1
231 splicing events in other mESC datasets and supported that several of these were
232 specifically enriched in mESC (Fig. S3f, Table S1).

233 Interestingly, visual inspection of the genome topology around the *Stag1* locus in
234 our 2i mESC and neural stem cell (NSC) Hi-C data [64] revealed that the *STAG1* gene
235 undergoes significant 3D reorganization as cells differentiate (Fig. S4). For example, the
236 *STAG1* TAD switches from the active to the repressive compartment during
237 differentiation, in line with the decrease in Stag1 levels during differentiation.
238 Furthermore, UMI-4C revealed changes to sub-TAD architecture corresponding to the
239 newly discovered mESC-enriched Stag1 TSSs and TTSs described above, suggesting
240 that 3D chromatin topology may play a role in facilitating the transcriptional diversity of
241 *STAG1* (Fig. S4). Together, our results point to a previously unappreciated diversity of
242 endogenous Stag1 transcripts in mESCs, prompting us to investigate the importance of
243 these for pluripotency and the nucleolus.

244

245 **Multiple Stag1 protein isoforms are expressed in mESCs.**

246 Stag1 transcript diversity was intriguing because many of the events were either specific
247 to mESC or enriched compared to MEFs and NSCs (Fig. S3d, f). Furthermore, the
248 transcript variants were predicted to produce STAG1 protein isoforms with distinct
249 structural features and molecular weights (Fig. 3d, S3g). For example, the truncation of
250 the N-terminus (e2/3Δ, e5Δ, e6 TSS and e7 TSS), and thus loss of the AT-hook (amino
251 acid 3-58), could impact STAG1 association with nucleic acids. Meanwhile, C-terminal
252 truncated Stag1 isoforms (altex22, i25 end, e31Δ) could affect STAG1-cohesin
253 interactions. It is noteworthy that the evolutionarily conserved Stag-domain ('SCD', AA
254 296-381) [30], shown to play a role in CTCF interaction [29], would be retained in all the
255 isoforms identified here.

256 Immunoprecipitation (IP) of endogenous STAG1 followed by WB revealed
257 multiple bands corresponding to the predicted molecular weights for several protein
258 isoforms and identified by mass spectrometry to contain Stag1 peptides (Fig. 3e, S3g,
259 Table S2). Similarly, multiple bands of expected sizes were reduced between naïve and
260 primed cells (Fig. S3h) and sensitive to Stag1 KD, alongside the canonical, full-length
261 isoform (Fig. 3f). Treatment of SA1^{NG_FKBP} mESCs with dTAG followed by WB of
262 chromatin-associated proteins with an antibody to the v5 tag further confirmed the
263 sensitivity of the isoforms to dTAG-mediated degradation (Fig. 3g). Thus, complex
264 transcriptional regulation in mESCs gives rise to multiple Stag1 transcripts and protein
265 isoforms with distinct regulatory regions and coding potential. Our discovery of such
266 naturally occurring isoforms offers a unique opportunity to define the functions of the
267 divergent N- and C-terminal ends of Stag1 in the context of the pluripotent state.
268
269 To study the functional consequences of the Stag1 isoforms on pluripotency and
270 nucleolar structure, we took advantage of our detailed understanding of Stag1 transcript
271 diversity to design custom siRNAs to selectively target, or retain specific isoforms (Fig.
272 4a). Alongside the siRNAs used in Figure 1 (SmartPool, SP), we designed siRNAs to
273 specifically target the SATS 5'UTR (esiSATS), the 5' end (siSA1-5p) or the 3' end
274 (siSA1-3p) of Stag1 mRNA (see Methods). We anticipated that the KD panels would not
275 completely abolish all Stag1 transcript variants, but rather change the relative
276 proportions, in effect experimentally skewing the levels of the N- and C-terminal ends of
277 Stag1 in cells. 3p siRNAs were predicted to downregulate full-length and N-term
278 truncated isoforms and retain C-term truncated isoforms, while 5p siRNAs would
279 specifically retain N-term truncated isoforms.
280 siRNAs to the 5p and 3p ends of Stag1 reduce full-length Stag1 mRNA and
281 protein with similar efficiency to SP KDs. esiSATS reduces Stag1 by ~30-50%,
282 indicating that the SATS TSS functions to enhance expression of Stag1 in naïve mESC
283 (Fig. 4b, S5a). We confirmed that Stag1 isoform proportions were altered upon siRNA
284 treatment using RNA-seq, RACE and immunoprecipitation. RNA-seq reads aligning to
285 Stag1 in the different siRNA treatments were quantified to represent the residual N-

286 terminal, middle and C-terminal read proportions (Fig. 4c). Residual reads in the SP and
287 3p KDs aligned predominantly to the N-terminus and were depleted from the C-
288 terminus. While the 5p KD had the least read retention in the N-terminus (Fig. 4c). In
289 parallel, we performed RACE to validate changes to the proportions of Stag1 isoforms.
290 5' RACE performed in mESC treated with 5p siRNA revealed downregulation of full-
291 length Stag1 transcript while several N-terminal truncated isoforms were upregulated
292 compared to untreated cells (Fig. 4d, left panel, blue arrows). Similarly, transcripts
293 terminating at the canonical 3' end of Stag1 are strongly reduced in the SP and 3p
294 siRNA KD samples and to a lesser extent in the 5p KD (Fig. 4d, red arrows), supporting
295 the expectation that residual transcripts in the 5p KD have C-terminal ends. Meanwhile,
296 the transcript terminating in i25 is substantially enriched upon 3p KD (Fig. 4d, right
297 panel, green arrows). Thus, the siRNA panel developed here provide us with a powerful
298 tool to modulate the proportion of the naturally occurring Stag1 isoforms in mESCs and
299 study their potential roles in pluripotency.

300 **A specific role for the Stag1 C-terminus in the maintenance of naïve pluripotency**
301 **transcriptome.**

302 We first quantified the effect of the Stag1 siRNA KDs on pluripotency gene expression.
303 qRT-PCR for Nanog expression and WB for Nanog protein levels revealed that the 3p
304 KD had a similar effect on Nanog to SP, with significant downregulation, while
305 surprisingly, the 5p KD did not reduce Nanog (Fig. S5b). We prepared biological
306 replicate RNA-seq libraries from the Stag1 3p, 5p and SATS siRNA KDs. We used
307 GSEA as before to probe for signatures of naïve or primed pluripotency. In support of
308 our previous results, reducing Stag1 levels by targeting the mESC-specific SATS
309 promoter leads to downregulation of the naïve pluripotency gene signature and
310 upregulation of the primed signature (Fig. 4e, S5c), reminiscent of the phenotype from
311 SP KD (Fig. 1e, f). We again observed a differential effect of the 3p and 5p KDs on
312 naïve and primed pluripotency signatures. A similar but more prominent loss of the
313 naïve signature was observed in 3p KD RNA-seq compared to SATS and SP, while

314 surprisingly, in 5p KD cells the naïve signature was unaffected compared to si scr
315 controls (Fig. 4e).

316 The distinct gene expression profiles of the 3p and 5p KDs were reflected in
317 differences in self-renewal. Cells treated with 3p siRNAs exhibited a significant loss of
318 self-renewal potential, consistent with the loss of the naïve pluripotency signature, with
319 only 20% of colonies exhibiting AP-staining compared to 30% of colonies in the SP KDs
320 (Fig. S5d), and an average reduction of the area occupied by AP+ colonies of 50%
321 compared to si scr controls (Fig. 4f). This was not evident in the 5p KD, where the effect
322 on self-renewal was more similar to si scr controls (Fig. 4f). Interestingly, unlike siRNA
323 to Stag1, esiSATS results in a variable effect on self-renewal (ranging from between 5-
324 35% reduction in AP+ area) (Fig. 4f), likely because the SATS TSS is expressed in the
325 most naïve cells of the population, the frequency of which varies significantly between
326 FCS populations. Our results further confirm the importance of Stag1 in self-renewal
327 and point to a specific role for the C-terminal of Stag1 in maintaining a naïve
328 pluripotency gene expression programme.

329 **The N-terminus of Stag1 supports nucleolar structure and function.**

330 The different effect on naïve pluripotency between the 3p and 5p KDs was surprising.
331 We therefore sought to re-examine the effect of our siRNA panel on the Stag1 bound
332 repeats LINE1 and rDNA (Fig. 2f, g). As we had not observed a significant difference
333 on steady state levels of repeats from our RNA-seq experiments, we instead purified
334 nascent RNA from mESCs treated with siRNAs. Both the KD and the nascent RNA
335 pull-downs were successful as revealed by qRT-PCR to Stag1 (Fig. 5a, b). Consistent
336 with our previous results, total Nanog RNA levels were significantly reduced in siSA1
337 SP and 3p KD but not in 5p KD. Interestingly, this trend was not observed in nascent
338 levels of Nanog RNA where the 3p KD does not have a significant effect, suggesting
339 that the C-terminus may be required for the stability of Nanog mRNA instead of its
340 transcription *per se* (Fig. 5a, b). Upon Stag1 SP KD, both steady state and nascent
341 levels of LINE1 RNA were modestly decreased (also Fig. S2f). While the 3p KD had a
342 20% reduction in LINE1 RNA expression, this was not maintained at steady state levels.

343 However, both nascent and total levels of LINE1 RNA were significantly reduced by 40-
344 50% of controls in 5p KD mESCs. These results were also observed for pre-rRNA, with
345 only the SP and 5p KD having significant effects on expression. Thus, the N-terminus
346 of Stag1 plays a distinct role in LINE1 and rDNA expression (Fig. 5a, b).

347 Given the effects on LINE1 and rRNA, we also assessed nucleolar structure and
348 function using our siRNA panel. mESC were pulsed with 5-ethynyl uridine (EU) which
349 becomes actively incorporated into nascent RNA and enables detection of newly
350 synthesized RNA. Samples for IF were co-stained with an antibody to NCL to
351 simultaneously quantify nucleoli number and changes in nascent RNA transcription.
352 Cells treated with scrambled siRNA showed a distinct nucleolar structure and the EU
353 signal could be seen throughout the nucleus, with a strong enrichment within the
354 nucleolus as expected from rRNA expression (Fig. 5c). While a significant reduction in
355 nascent RNA signal was observed in all KD conditions compared to scrambled controls
356 (Fig. S5e), by IF, we observed a distinct effect on nascent RNA levels within the
357 nucleolus in the 5p KD. While the medians between the three siSA1 KDs were not
358 dramatically different, the effect of the 5p KD on nucleolar RNA signal distribution was
359 significantly different from the 3p KD (Fig. 5d). This result was consistent with the qRT-
360 PCR analysis of nascent pre-rRNA levels (Fig. 5b) and with the significant effect on
361 NCL foci number in 5p KD mESCs (Fig. 5e). Consequently, we also observed changes
362 to global translation by assessing the incorporation of L-homopropargylglycine (HPG),
363 an amino acid analogue of methionine into mESC using FACS analysis. HPG
364 incorporation was significantly reduced in SP and 5p siRNA treated mESCs compared
365 to scrambled control (32% and 35% of si Scr) (Fig. 5f, S5f). We did observe a modest
366 effect on global nascent translation in 3p KD treated cells (16% of si scr), although this
367 was not significantly different from scrambled control. Our results reveal distinct roles for
368 the N- and C-termini of Stag1 in nucleolar structure and function and pluripotency gene
369 expression, respectively.

370 The effects observed on rRNA levels and nucleolar function were not associated
371 with changes to expression of ribosome subunit expression (Fig S5g). Thus, we

372 considered whether the regulation of LINE1 expression by the N-terminus of Stag1
373 influenced nucleolar structure via the NCL/Trim28 complex (Fig. 2l). To investigate this,
374 we took advantage of our Stag1^{NG_FKBP} mESCs. dTAG treatment can only degrade
375 isoforms containing the FKBP tag inserted into the canonical C-terminal end. Thus
376 Stag1^{NG_FKBP} mESCs treated with dTAG should enrich for SA1$^{\Delta C}$ isoforms which contain
377 an N-terminus. Indeed, immunoprecipitation of STAG1 using an antibody which
378 recognizes an N-terminal epitope reveals the presence of several N-terminal-enriched
379 SA1ΔC isoforms (Fig. 5g, green arrows). WB of this IP material revealed a reduction in
380 the ability of SA1ΔC to interact with the cohesin subunits Rad21 and Smc3, despite
381 similar levels in the input of dTAG treated cells. Meanwhile, the interaction with NCL
382 was increased in same lysate (Fig. 5g). Taken together, our results are supportive of the
383 different ends of Stag1 interacting with different protein partners to co-ordinately
384 regulate pluripotency.

385

386 **The N-terminus of Stag1 suppresses the totipotent state.**

387 In addition to promoting rRNA synthesis and self-renewal in mESC, the LINE-
388 1/NCL/Trim28 complex represses a transcriptional program specific to totipotent cells in
389 the two-cell (2C) stage of development, termed two-cell-like (2C-LC) [56]. The
390 phenotypes of the 5p KD, namely reduced rRNA and LINE-1 expression, reduced
391 translation and aberrant nucleolar function, pointed towards possible conversion of cells
392 into a 2C-LC state. We therefore tested whether Stag1, and specifically the N-terminal
393 end, play a role in totipotency.

394 We first investigated whether 2C-L cells which naturally arise within mESC
395 populations express Stag1NΔ isoforms. To formally address this, we obtained mESCs
396 expressing a Dox-inducible *Dux-HA*-expression construct together with a MERVL-linked
397 GFP reporter [65]. Dux is a 2C-specific transcription factor which binds to MERVL
398 elements to activate expression (Hendrickson et al., 2017). We induced *DuxHA*-
399 expression in the MERVL-GFP mESC and performed 5' RACE as before on sorted

400 GFP+ (2C-L) and GFP- cells (Fig. 6a). We enriched several of the previously identified
401 N-term truncated Stag1 transcripts in the GFP+ population including e2/3Δ and e5Δ
402 isoforms (Fig. 6a, blue arrows). Importantly, we also identified a transcript starting at e7,
403 similar to the one previously found in 5p KD mESC (Fig. 6b, 3a, b). Remarkably
404 however, the sequence preceding the TSS in e7 in *Dux*-induced cells was an MT2-
405 MERVL element, creating a chimeric, LTR-driven Stag1 transcript, reminiscent of other
406 LTR-transcripts specifically expressed in the 2C-L state.

407 2C-LCs are a rare subpopulation which spontaneously arise in mESC cell
408 cultures and exhibit unique molecular and transcriptional features [43,66,67]. Given that 2C-
409 LCs expressed several N-term truncated Stag1 isoforms, we investigated whether these
410 in turn supported the maintenance or emergence of that state. We treated mESCs with
411 the panel of siRNAs and used RT-qPCR to test expression of candidate genes. We
412 found that Dux, and consequently MERVL and other markers of the totipotent 2C-L
413 state, Gm6763, AW822073 and Gm4981 are strongly upregulated by 5p KD (Fig. 6c, d,
414 S6a). Notably, all 2C-L genes analysed remained unchanged in 3p KD conditions with
415 a modest upregulation in SP KD. Further, GSEA using a published 2C gene set [56]
416 revealed a specific enrichment among the upregulated genes in 5p KDs that was not
417 observed in 3p KDs (Fig. 6e, S6b), consistent with the different ends of Stag1 targeting
418 different RNA pools.

419 To functionally validate the expression results, we returned to the Dox-inducible
420 *Dux-HA*, MERVL-GFP mESCs [65] and used flow cytometry to directly measure the
421 number of GFP-positive cells in our different Stag1 KD conditions (Fig. 6f, g). Chaf1 is a
422 chromatin accessibility factor previously shown to support conversion of mESC towards
423 totipotency [43]. In support of the upregulation of the 2C-LC gene set in 5p KD mESCs,
424 we observed an 8-9-fold increase in the proportion of GFP-positive cells in 5p KD
425 conditions compared to scramble treated controls, similar to the published effect of
426 Chaf1 KD (Fig. 6f, g). There was a modest, but insignificant increase in GFP+ cells
427 upon SP KD and no effect upon 3p KD. mESC treated with both Chaf1 and 5p siRNAs
428 had an additive effect on the proportion of GFP-positive cells, suggesting that the two

429 proteins function in complementary pathways for conversion towards totipotency. Thus,
430 2C-LCs express N-term truncated Stag1 isoforms which in turn support the
431 maintenance or emergence of that state through rRNA repression and nucleolar
432 changes. Together our results reveal a new and specific role for the N-terminus of
433 STAG1 in the regulation of the totipotent state.
434

435 **DISCUSSION**

436 Most studies of cohesin function focus on the core trimer, despite the fact that it is the
437 regulatory Stag subunit that are pan-cancer targets [3] and have clear roles in cell identity
438 control [2]. How these proteins contribute to cohesin's functions, why cells have
439 diversified them so extensively and how their mutations lead so often to disease are
440 poorly understood. Here we reveal a novel role for Stag1, and in particular its unique N-
441 terminal end, in regulating nucleolar integrity and 2C repression to maintain mESC
442 identity. It has been known for a long time that several Stag paralogs exist in
443 mammalian cells and that they have non-reciprocal functions with respect to
444 chromosome structure and cohesion. By dissecting the diversity of naturally occurring
445 Stag1 isoforms in mESCs, we have shed new light not only on the unique divergent
446 ends of the Stag paralogs but also the critical role that their levels play in cell fate
447 control. Our results highlight the importance of careful understanding of chromatin
448 regulators in cell-specific contexts.

449 Stag1 knockout (Stag1$^{\Delta/\Delta}$) ESCs give rise to mice which survive to E13.5 [33,68]. At
450 first this observation seems at odds with our report that Stag1 is required for
451 pluripotency. However, our observations may in fact explain why the Stag1$^{\Delta/\Delta}$ mouse
452 model does not exhibit early embryonic lethality. In this model, only the 5' region of
453 Stag1 was targeted, meaning that the Stag1 isoforms lacking the N-terminus may still
454 be retained in the targeted ESCs. This is consistent with our results showing that 5p KD
455 cells have not lost their ability to self-renew nor is their pluripotency gene signature
456 affected. It further suggests that changes to the nucleolus may exist in these cells.

457 The nucleolus is held together by liquid–liquid phase separation (PS), which is
458 driven by the association of rDNA with nucleolar proteins and is dependent on continual
459 rRNA synthesis [37,38]. However, in one- to two-cell embryos, nucleoli lack distinct
460 compartments, exhibit low rRNA synthesis and low translation [69]. Similarly, changes to
461 rRNA synthesis or nucleolar PS are sufficient to convert ESCs towards the 2C-LC state,
462 either through Dux dissociation from the nucleolar periphery and consequently its de-
463 repression [44] or p53-mediated nucleolar stress [47]. Other proteins including the
464 NCL/TRIM28 complex [56] and nucleolar LIN28 [48] have been shown to contribute to
465 nucleolar integrity and repress DUX expression. In this context, our results position
466 Stag1, and specifically its N-terminal end, as a novel regulator of the 2C-ESC transition
467 through the control of nucleolar integrity. Stag1 is localised to the nucleolar periphery
468 and interacts with the nucleolar proteins NCL/TRIM28 as well as being bound to and
469 supporting rDNA and LINE-1 element expression. Our results suggest that the N-
470 terminus of Stag1 plays a specific role in repressing conversion to 2C state. Stag1 may
471 contribute to nucleolar structure and function via both the regulation of rRNA expression
472 as well as by supporting nucleolar PS through interactions with nucleolar regulators. In
473 this context, modulating the availability of the N- or C-terminus of Stag1 may be a way
474 in which ESCs impact nucleolar structure and function and thus cell identity. Our results
475 also point to the different ends of Stag1 interacting with different protein partners since
476 mESCs retaining the C-terminus of Stag1 do not exhibit changes to the nucleolus and
477 do not convert into 2C-LCs. This is also supported by the different gene expression
478 programmes affected in the KDs that select for N-termΔ or C-termΔ isoforms. It may in
479 fact be quite important for ESCs to express a diversity of alternative Stag1 isoforms to
480 support plasticity of nucleolar structure and a range of cell fate options from totipotency
481 to primed pluripotency.

482 Finally, Stag genes are commonly mutated in cancers [3]. Our results point to
483 misregulation of Stag proteins as leading to epigenetic misregulation, not necessarily
484 only through changes to TADs and protein coding genes, but support a role for cell fate
485 changes as a result of hierarchical changes to chromatin organization, nucleolar

structure and function and repeat misregulation. Careful analysis of Stag2-mutant cancers should shed light on these and deliver new insights into cancers that harbour these mutations.

Acknowledgments

This work would not be possible without the support of a Senior Research Fellowship from the Wellcome Trust awarded to S.H. (106985/Z/15/Z). We would like to thank Sally Lowell and Mattias Malaguti for advice throughout the project. We are grateful to the members of the Hadjur lab for critical discussions and reading of the manuscript. We thank M. Irima for help with VAST-tools pipelines; B. Cairns for the inducible Dux-HA, MERVL-GFP ESCs; W.Reik for a second MERVL-reporter ESC line; H. Rowe for advice on 2C-LC cells and repeat analysis. Thank you to Y. Guo and J. Manji in the Cancer Institute CRUK Centre FACS and Imaging core facilities for their invaluable assistance.

Author Contributions

D.P. and S.H. conceived the project. D.P. designed and performed all the experiments on ESCs with assistance from S.W. S.W. performed all protein analysis, generated the SA1-NG-FKBP ESC line, performed the Spinning Disk microscopy and helped with the siRNA knockdown experiments. W.V. performed all bioinformatic analyses with the exception of the Stag1 enrichments at repeat elements, which was done by M.B. P.D. and S.P. provided advice on CRISPR targeting. D.P. and S.H. formatted all figures and wrote the manuscript with input from all authors.

Declaration of Interests

The authors declare no competing interests.

511 **FIGURE LEGENDS**

512 **Figure 1. STAG1 is required for naïve pluripotency in mouse ESCs.**

513 a) Log2 fold change of Stag1 (SA1) and Stag (SA2) gene expression assessed by qRT-PCR
514 during *in vitro* mESC cell differentiation towards EpiLC. Multiple primer pairs were used for SA1
515 (blue) and SA2 (purple) mRNA (see box). Data are derived from two biological replicates.

516 b) Whole cell protein extracts (WCL) from naïve mESC and EpiLCs and analysed by western
517 blot (WB) for levels of SA1, SA2 and Smc3. H3 serves as a loading control.

518 c) WB analysis of SA1 levels in WCL and chromatin fractions upon treatment with scrambled
519 control siRNAs (si scr) or SmartPool SA1 siRNAs (siSA1) for 24hr in naïve mESC cells. Tubulin
520 (Tub) and H3 serve as fractionation and loading controls.

521 d) Left, relative expression of Nanog mRNA by qRT-PCR in naïve mESCs upon treatment with
522 si scr, esiLuciferase control or siSA1. Data are from 8 biological replicates. Right, Mean
523 fluorescence intensity (MFI) of Nanog protein assessed by Immunofluorescence (IF) in naïve
524 mESCs treated with same siRNAs as before. Cells were counterstained with DAPI. Data is
525 n>100 cells/condition across 2 biological replicates. Whiskers and boxes indicate all and 50% of
526 values, respectively. Central line represents the median. Asterisks indicate a statistically
527 significant difference as assessed using two-tailed t-test. * $p<0.05$, ** $p<0.005$, *** $p<0.0005$,
528 **** $p<0.0001$, ns = not significant.

529 e) Volcano plot displaying the statistical significance (-log2 p-value) versus magnitude of change
530 (log2 fold change) from RNA-sequencing data produced in mESCs treated with siscr or siSA1
531 for 24hrs. Data is from 3 biological replicates. Vertical blue dashed lines represent changes of 2-
532 fold. Selected genes associated with cohesin, pluripotency and differentiation have been
533 highlighted in red.

534 f) Enrichment score (ES) plots from Gene Set Enrichment analysis (GSEA) using curated naïve
535 or primed pluripotency gene sets (see Methods). Negative and positive normalized (NES)
536 enrichment scores point to the gene set being over-represented in the top-most down- or up-
537 regulated genes in SA1 KD mESC, respectively. Vertical bars refer to individual genes in the
538 gene set and their position reflects the contribution of each gene to the NES.

539 g) Area occupied by AP+ colonies in mESCs treated with si scr and si SA1 from three
540 independent biological replicates where n>50 colonies/condition were counted.
541

542 h) CRISPR/Cas9 was used to knock-in a NeonGreen-v5-FKBP tag on both alleles of
543 endogenous Stag1 at the C-terminus ($SA1^{NG\text{-}FKBP}$). The resultant Stag1 protein is 42kDa larger.
544 Shown also are known features of SA1 including the N-terminal AT-hook (AT) and the stromalin
545 conserved domain (SCD). WB analysis of SA1and Nanog levels in a targeted mESC clone after
546 treatment with DMSO or dTAG. Tubulin (Tub) serves as a loading control.
547

548 i) Analysis of the area occupied by AP+ colonies as above but in WT or SA1$^{NG\text{-}FKBP}$ mESC
549 treated with DMSO or dTAG. Data is from three independent biological replicates where n>50
550 colonies/condition were counted.
551

552 **Figure 2. Stag1 is localised to and impacts both euchromatin and heterochromatin**
553 **compartments.**

554 a) Live-cell Spinning Disk confocal images of two SA1$^{NG\text{-}FKBP}$ mESCs counterstained with
555 Hoechst. Arrows indicate notable regions of overlap of SA1 and Hoechst, including at Hoechst-
556 dense foci and at the nucleolar periphery. *NB* Puncta within the nucleoplasm can also be
557 observed.

558 b) Imaris quantification of the MFI of SA1-NeonGreen within the nucleus (light grey) or Hoechst-
559 dense foci (dark grey). Quantifications and statistical analysis were done as above. Data is from
560 two independent experiments, n>50 cells/condition. AU, arbitrary units.

561 c) Distribution of Hoechst MFI from SA1$^{NG\text{-}FKBP}$ mESCs treated with DMSO (green) or dTAG
562 (black). Data is from n>100 cells/condition.

563 d) Imaris quantification of the volume of Hoechst foci in SA1$^{NG\text{-}FKBP}$ mESC treated with DMSO
564 (green) or dTAG (white). Quantifications and statistical analysis were done as above. Data is
565 from two independent experiments, n>50 cells/condition. AU, arbitrary units.

566 e) Number of copies of each repeat family that overlap a SA1 ChIP-seq peak and the
567 enrichment of binding over random. Shown in red are the repeats which have significant
568 enrichment, with a subset of these labelled.
569
570 f) Profiles of the mean enrichment of SA1 ChIP-seq at select TE repeat families. Shown are
571 full-length elements of the indicated SINE, LINE and LTR families. Two SA1 ChIP replicates are
572 shown in blue.

573 g) Top, cartoon of the consensus Mus musculus ribosomal DNA (rDNA) (GenBank:
574 BK000964.3), showing the ribosomal genes and the intergenic spacer (IGS) region which
575 contains several SINE elements (Red, B2_Mm2; Green, B3). Bottom, Stag1 ChIP replicates and
576 INPUT as in f) above, aligned to this region.

577 h) Representative confocal images of MFI of SA1-NeonGreen and Nucleolin (NCL) assessed by
578 IF in SA1$^{NG\text{-}FKBP}$ mESCs treated with DMSO or dTAG and counterstained with DAPI.

579 i) Imaris quantification of the MFI of SA1-NeonGreen from h) within the nucleus or NCL foci in
580 DMSO and dTAG conditions. Quantifications and statistical analysis were done as above. Data
581 is from two independent experiments, n>50 cells/condition. AU, arbitrary units.

582 j) Distribution of NCL MFI from SA1$^{NG\text{-}FKBP}$ mESC treated with DMSO (green) or dTAG (black).
583 Data is from n>100 cells/condition.

584 k) Imaris quantification of the number of NCL foci in wildtype mESC treated with si scr (grey) or
585 siSA1 SP siRNAs (red) and in the SA1$^{NG\text{-}FKBP}$ mESC clone treated with DMSO (green) or dTAG
586 (white). Quantifications and statistical analysis were done as above. Data is from two
587 independent experiments, n>50 cells/condition. See also Figure S2.

588 l) Chromatin immunoprecipitation of SA1 and IgG from wildtype mESCs and WB for SA1, NCL
589 and Trim28. Blue arrows indicate multiple immunoreactive bands to SA1.

590

591 **Figure 3. Stag1 undergoes widespread transcriptional regulation in mESCs.**

592 a) 5' Rapid Amplification of cDNA ends (RACE) for SA1 in naïve mESC and EpiLCs. Left gel;
593 red star indicates SATS TSS and red arrow indicates canonical (can) TSS. Right gel; red arrow
594 indicates full length Stag1 with both SATS and can TSSs; dark blue arrow indicates alternatively
595 spliced variants arising from skipping of exons in the 5' region; light blue arrows indicate the
596 TSSs at exon 6 (e6) and exon 7 (e7). Arrows indicate bands which were cloned and sequenced.
597 See also Figure S3.

598 b) The 5' RACE fragment that identified a new TSS at exon 7 spliced directly to a sequence in
599 trans carrying regulatory elements.
600
601 c) 3' RACE for SA1 in naïve mESCs. Red arrow indicates canonical full-length end; green arrow
602 indicates end in i25. Arrows indicate bands which were cloned and sequenced. See also Figure
603 S3.
604
605 d) Top, schematic of the *STAG1* gene annotation in mm10. The identified TSS and TTSs from
606 RACE are indicated. Bottom, aligned sequence clones from the PCR mini-screen and their
607 predicted impact on the SA1 protein (grey box, right). Green arrows and red bars within the
608 transcripts indicate start of the coding sequence and the TTS respectively. Shown also are the
609 regions which code for the AT hook and the stromalin conserved domain (SCD).

610 e) Schematic of the PacBio sequencing methodology (see methods for full description). Select
611 transcripts sequenced on the PacBio platform, including many isoforms already discovered
612 using RACE and PCR cloning methods above. See also Figure S3.
613
614 f) WB analysis of endogenous, chromatin-bound SA1 protein isoforms from mESCs and g) upon
615 treatment with si scr and siSA1. H3 serves as a loading control.

616 h) Chromatin immunoprecipitation for the v5 tag in SA1$^{NG\text{-}FKBP}$ mESCs treated with DMSO or
617 dTAG to degrade SA1. *NB.* SA1 bands run 42kDa higher due to the addition of the tag.

618 **Figure 4. Fluctuations in the levels of the Stag1 isoforms skews cell fates.**

619 a) Schematic of the siRNA pools used in this study. esiRNA SATS represents 'enzymatically-
620 prepared' siRNAs (see Methods).

621 b) WB analysis of SA1 levels in mESC WCL after no treatment (UT), or upon si scr, si SA1 SP,
622 si SA1 3p, si SA1 5p or esi SATS treatment. Tubulin serves as a loading control. The
623 percentage of knockdown (KD) of SA1 signal normalised to Tubulin is shown.

624 c) RNA-seq reads (TPM, transcripts per million) aligning to sectioned Stag1 in datasets from the
625 various siRNA pools, shown as relative to untreated mESC RNA-seq. N-terminal reads include
626 SATS and exons 1-8, Mid reads include exons 12-19 and C-terminal reads include exons 20-25
627 and exons 26-34. *NB.* the change in read proportions in the different KD treatments.

628 d) Left gel, 5' and Right gel, 3' RACE for SA1 in mESC treated with the indicated siRNAs.
629 Arrows indicate bands which were cloned and sequenced and colour-coded as before.

630 e) Enrichment score (ES) plots from GSEA using the naïve and primed gene sets as in Fig. 1e
631 and RNA-seq data from the indicated siRNA treated mESC samples.

632 f) Area occupied by AP+ colonies in mESC treated with the siRNA panel from three
633 independent biological replicates. n>50 colonies/condition were counted.

634

635 **Figure 5. The N- and C-terminal ends of Stag1 regulate expression in different genomic**
636 **compartments.**

637 Relative expression of Stag1, Nanog, LINE1-T and pre-rRNA by qRT-PCR in mESC after
638 treatment with the siRNA panel. Shown are a) total and b) nascent RNA levels. Data is
639 represented as mean ± SEM and statistical analysis as before. Data is from three independent
640 experiments.

641 c) Representative confocal images of IF to NCL and nascent RNA in siRNA-treated mESC
642 labelled with EU-488. Nuclei were counterstained with DAPI.

643 d) Imaris quantification of the MFI of nascent RNA (EU) within the nucleoli from (c), as defined
644 by a mask made to the NCL IF signal. Quantifications and statistical analysis were done as
645 above. Data is from two independent biological replicates. n>50/condition, except for siSA1 5p
646 where n>35.

647 e) Imaris quantification of the number of NCL foci in siRNA-treated mESCs. Quantifications and
648 statistical analysis were done as above. Data is from two independent experiments, n>50
649 cells/condition.

650 f) Analysis of global levels of nascent translation by measuring HPG incorporation using Flow
651 cytometry and analysed using FloJo software. Shown is the quantification of the change in EU
652 incorporation relative to si scr treated cells. Data are from four biological replicates.

653 g) Chromatin immunoprecipitation using an N-terminal Stag1 antibody in SA1$^{NG\text{-}FKBP}$ mESC
654 treated with DMSO or dTAG. Green arrow indicates residual C-terminal truncated Stag1
655 isoforms. Shown also are WB for the core cohesin subunits Rad21 and Smc3 and NCL.

656

657 **Figure 6. Stag1 N-terminus protects against conversion of ESCs to totipotency.**

658 a) 5' RACE for Stag1 in Dux-HA MERVL-GFP mESCs with and without sorting for GFP+ cells.
659 Arrows indicate bands which were cloned and sequenced and colour-coded as previously
660 described.

661 b) Sequence of the 5'RACE product identifying a novel Stag1 TSS from (a) with direct splicing
662 of exon7 to an MT2_MERVL element.

663 c) Relative expression of several 2C-LC markers in total RNA by qRT-PCR in mESC after
664 treatment with the siRNA panel. Data is represented as mean ± SEM and statistical analysis as
665 before. Data is from six independent experiments.
666
667 d) Relative expression of MERVL repeat element by qRT-PCR in mESC after treatment with the
668 siRNA panel. Shown are total (left) and nascent RNA (right) levels. Quantifications and
669 statistical analysis as before. Data is from five biological replicates. *NB,* nascent RNA levels are
670 shown relative to si scr control.

671 e) Enrichment score (ES) plots from GSEA using a published 2C-L gene set and RNA-seq data
672 from the 3p and 5p siRNA treated mESC samples used in Figure 4.

673 f) Representative FACS analysis of the proportion of mESCs expressing a MERVL-GFP
674 reporter in the different siRNA treated cells and including siRNA to Chaf1 as a positive control.
675 Percentage of MERVL-GFP+ cells based on Flo-Jo analysis is shown in red.

676 g) Proportion of MERVL-GFP+ cells in the different siRNA conditions relative to the siChaf1
677 positive control. Data is represented as mean ± SEM and statistical analysis as before and is
678 from four independent experiments.

679 **METHODS**

680 **Embryonic stem cell culture and siRNA-mediated knockdown.**

681 Male mouse E14 embryonic stem cells (mESC) were cultured in serum (FCS) or naïve (2i)
682 conditions. Serum-cultured cells were grown on 0.1% gelatin-coated plates in GMEM, 10% FCS
683 (Sigma), NEAA, Na Pyruvate, 0.1 mM ßMercaptoethanol (BMe), Glutamax, and freshly added
684 LIF (1:10,000). 2i-cultured cells were grown on plates coated with Fibronectin, in
685 DMEM:F12/Neurobasal 1:1, KnockOut Serum Replacement, N2, B27, Glutamax, 1μM
686 PD0325901, 3μM CHIR9902, 0.1 mM BMe, and freshly added LIF as above. DuxHA/MERVL-
687 GFP cells were cultured in 2i conditions. siRNAs were purchased from Horizon Discovery
688 (previously Dharmacon) or Sigma (for 'enzymatically-derived' esiRNAs). siRNA knockdowns
689 (KDs) were performed for 24hr with the exception of those in Figure 5 which were performed for
690 72hr. Knockdowns were performed in 6-well plates where 200,000 cells were seeded for 72 hr
691 KDs, and 400,000 for 24 hr KD. 50pmol siRNAs were transfected using RNAiMax Lipofectamine
692 at the time of seeding, and after 48 hrs for 72hr timepoints. Two siRNA controls were used,
693 scrambled (scr) was D-001810-10 and Luciferase (esiLuc) control purchased from Sigma. siSA1
694 'SmartPool' (SP) was derived from equimolar ratios of commercial siRNAs (D-041989-02, -04, -
695 05, -06, -07, -08). siSA1 5p was a custom Duplex siRNA sequence
696 (AGGAGCAGGUCGUGGAAGAUU). siSA1 3p was derived from equimolar ratios of commercial
697 siRNAs J-041989-05, -07, -08. esiRNA to SATS was purchased from Sigma as a custom-made
698 product to the entire SATS 5'UTR (mm10 chr9:100,597,794-100,598,109).

699

700 **qRT-PCR analysis**

701 Total RNA was isolated using Monarch RNA prep kit (NEB). Reverse transcription was
702 performed on 0.5 μg DNase-treated total RNA using Lunascript RT (NEB) in 20μl reactions.
703 qPCR was performed using 2x SensiFAST SYBR No-ROX kit (Bioline) in 20 μl reactions using
704 1μl of RT reaction as input and 0.4μM each primer.

705

706 **Alkaline Phosphatase (AP) assay and quantification**

707 Cells were seeded in 6 well plates and transfected with siRNAs at the time of plating as above.
708 After 24 hrs, cells were collected for RNA isolation and KD efficiency analyzed by qRT-PCR.
709 Cells from each condition were counted and 1,000 cells per well seeded into a new 6-well plate.
710 Cells were re-transfected after 48 hrs using 5 pmol of siRNAs. Cells were fed every day. Four

711 days after seeding cells at clonal density, the cells were assayed for alkaline phosphatase (AP)
712 expression using StemTAG Alkaline Phosphatase staining kit (Cell Biolabs CBA-300). AP
713 stained cells were imaged in 6-well plates using a M7000 Imaging System (Zeiss) with a 4X
714 objective and a Trans-illumination brightfield light source. For quantification, AP-high and AP-
715 low colonies from each condition were counted. Area occupied by AP-high colonies was also
716 measured using ImageJ, and plotted as fraction of total area of all colonies.
717
718 **RACE (Rapid Amplification of cDNA Ends) and PCR mini screen**
719 RACE was performed using GeneRacer kit (RLM RACE, Invitrogen L1500). 2μg of total RNA
720 was used as input. Final products were amplified by nested PCR, using Kapa 2x MasterMix.
721 First PCR was done in a 50μl reaction using 1μl RT as input, 25 cycles. DNA was purified using
722 Qiagen PCR Purification kit, and nested PCR was performed on a tenth of the first PCR for 30
723 cycles. Viewpoint for 5'RACE was in exon 2 (Fig 3A) or exon 8 (Fig 3B) of Stag1. Viewpoint for
724 3'RACE was in exon 23 (Fig 3C). RACE primer details can be found in Table S3. PCR products
725 were excised from the gel, A-tailed using Klenow exo- (NEB) and cloned into pCR4-TOPO
726 vector (Invitrogen). At least three clones were sequenced per PCR product. For the PCR Mini-
727 Screen, forward primers at either SATS or canonical 5' UTR were used with reverse primers
728 either at the end of Stag1 canonical coding sequence, or at the end of coding sequence in intron
729 25 (see Table S3). PCR was performed using Kapa 2x MasterMix. DNA was excised from the
730 gel, A tailed, and cloned into pCR4-TOPO. At least six clones per PCR product were Sanger-
731 sequenced. Sequences from the PCR Mini-screen were aligned using Minimap2 (2.14-r884) in
732 'splice' mode to ensure long read splice alignment (Fig 3D and S3A).
733
734 **PONDR Predictions**
735 Internally disordered regions were predicted using VSL2 predictor at http://www.pondr.com.
736
737 **CRISPR-Mediated Stag1 Knock-in Cell Line Generation**
738 The guide RNA targeting Stag1 3' terminal coding region was designed using Tagin Software
739 (http://tagin.stembio.org) and purchased from IDT. Lyophilised gRNA was rehydrated in RNA
740 duplex buffer (100μM). The single stranded oligodeoxynucleotides (ssODN) encoding
741 mNeonGreen (mNG)-V5-FKBP12^{F36V} and the left and right homology arms was designed using
742 the software tool ChopChop (https://chopchop.cbu.uib.no) and purchased as a High-Copy Amp-
743 resistant plasmid from Twist Bioscience. 2.2μl gRNA (100μM) was mixed with 2.2μl tracrRNA

744 ATTO 550nm (IDT) and annealed together. The RNA duplex was then incubated with 20μg S.p
745 Cas9 Nuclease V3 (IDT) for 10min at room temperature and stored on ice prior to transfection.
746 Linearised KI sequence was mixed with 100% DMSO and denatured at 95°C for 5min. The
747 ssODN was plunged immediately into ice. The RNP complex was mixed with confluent 2i-grown
748 ES cells re-suspended in P3 transfection buffer (Lonza) before being transferred to an
749 electroporation microcuvette well (Lonza). Transfection was performed using a 4D Amaxa
750 electroporator. Post-nucleofection, the cells were seeded into a fibronectin-coated 6 well plate
751 with fresh ESC media. The media was changed daily for four days before being expanded into a
752 T75 flask. Confluent ESC were FACS sorted for GFP+ population (BD FACS Aria Fusion Cell
753 Sorter) and sparsely seeded into 10 cm plates. Clones were manually picked into 96 well plates
754 and expanded for selection by v5 IF, genotyping and Sanger sequencing.
755
756 **Dox-inducible Stag1-GFP isoform cell lines**
757 Stag1 isoforms were cloned into pCW57.1 vector (Addgene 41393), modified using Gibson
758 assembly to include an EGFP tag at the 3'end of the Gateway cassette, using Gateway
759 recombination by LR clonase. For primers used to clone the isoforms see Supplementary Table
760 S3. Plasmids were transfected into 2i-grown ESCs using Lipofectamine 3000 and cells grown in
761 Puromycin-supplemented media (1μg/ml) for ten days to make stable lines. Isoform expression
762 was induced using 2μg/ml Doxycycline for 24 hrs, and the population enriched for GFP-positive
763 cells using FACS. For IF experiments, isoforms were induced by adding Dox for 48 hours.
764
765 **Protein Lysates, Fractionations and Western blotting.**
766 Whole cell lysates (WCL) were collected by lysis in RIPA buffer (150mM NaCl, 1% NP-40
767 detergent, 0.5% Sodium Deoxycholate, 0.1% SDS, 25mM Tris-HCl pH 7.4, 1mM DTT) and
768 sonicated at 4°C for x5 30 second cycles using Diagenode Bioruptor. Insoluble material was
769 pelleted and the supernatant lysate was quantified using BSA Assay (Thermo Scientific). For
770 cellular fractionations, a cellular ratio of $5x10^6$ cells/80μl buffer was maintained throughout the
771 protocol. Cells were re-suspended in Cell Membrane Lysis Buffer (0.1% Triton X, 10mM HEPES
772 pH 7.9, 10mM KCl, 1.5mM MgCl2, 0.34M sucrose, 10% glycerol, 1mM DTT), incubated on ice
773 for 5min and centrifuged for 5min at 3700rpm to collect the cytoplasmic sample. The pellet was
774 washed and then re-suspended in Nuclear Lysis Buffer (3mM EDTA, 0.2mM EGTA, 1mM DTT)
775 and incubated on ice for 1 hr. Nuclear lysis was aided by sonication with a handheld
776 homogeniser (VWR) for 10sec at 10min intervals. The nucleoplasmic supernatant and

777 chromatin pellet were separated by centrifugation at 9000rpm for 10min at 4°C. The chromatin
778 pellet was re-suspended in 160μl 2X Laemmli Buffer (Bio-Rad). Equal volumes of each fraction
779 were used for Western Blotting (WB). Cytoplasmic and nucleoplasmic protein samples were
780 diluted in 2X Laemmli Buffer and boiled for 5min at 95°C, then loaded on a 4-20% SDS-PAGE
781 gel (Bio-rad) or a 3-8% Tris Acetate gel (Invitrogen). Proteins were wet transferred onto a PDVF
782 membrane (Millipore) and assessed for successful transfer with Ponceau Red (Sigma). The
783 membrane was blocked with 10% milk and incubated with primary antibodies in 1% milk, 0.1%
784 Tween-PBS overnight at 4°C. Membranes were imaged with SuperSignal West Femto
785 Maximum Sensitivity (Thermo) on an ImageQuant.
786
787 **Chromatin Co-Immunoprecipitation (co-IP)**
788 Cells were re-suspended in 0.1% NP-40-PBS (1ml/1x10^7 cells) with 1X Protease Inhibitors
789 (Roche) and 1mM DTT, and centrifuged at 1500rpm for 2min at 4°C. The pellet was re-
790 suspended in Nuclear Lysis Buffer (3mM EDTA, 0.2mM EGTA, 1X Protease Inhibitors, 1mM
791 DTT), vortexed for 30sec before being incubated on a rotator for 30min at 4°C and centrifuged
792 at 6500g for 5min at 4°C to isolate the glassy chromatin pellet. This was re-suspended in High
793 Salt Chromatin Solubilisation Buffer (50mM Tris-HCl pH 7.5, 1.5mM MgCl2, 300mM KCl, 20%
794 glycerol, 1mM EDTA, 0.1% NP-40, 1mM Pefabloc, 1X Protease Inhibitors, 1mM DTT) with
795 Benzonase (Sigma) (6U/1x10^7) and incubated on rotator for 30min at 4°C. Chromatin was
796 digested with 3x 10sec sonication at 30% intensity with a Vibra-Cell probe. The supernatant was
797 collected by centrifugation at 1300rpm for 30min at 4°C, and then diluted to 200mM KCl
798 concentration with no KCL buffer. 30μl of Dynabeads (Invitrogen) were used per co-IP. Beads
799 were washed 2x in 200mM KCl IP Buffer, re-suspended in IP Buffer with 10μg of the IP
800 antibody, or an IgG-containing serum to match the species of the IP antibody and placed on
801 rotator for 5h at 4°C. Beads were washed 3x in IP buffer and then incubated in 1mg chromatin
802 lysate on a rotator overnight at 4°C. The beads were washed, re-suspended in 2X Laemmli
803 Buffer (Bio-Rad), boiled for 10min at 95°C and used for WB as above.
804
805 **Immunofluorescence and Microscopy**
806 ESCs were cultured on fibronectin or gelatin-coated cover glass in 6-well plates. Cells were
807 fixed in 4% Paraformaldehyde for 5min and incubated in 0.1% Triton X-PBS for 10min before
808 being washed and blocked in 10% FCS-PBS for 20min. Primary antibodies were diluted in 10%
809 FCS, 0.1% Saponin (Sigma) and incubated overnight at 4°C. The next day, the cells were

incubated with an Alexa fluorophore-conjugated secondary antibody diluted in 10% FCS, 0.1% Saponin for 1 hr at room temperature, washed and mounted on cover slides with ProLong Diamond Antifade Mountant with DAPI (Invitrogen). Z-stacks imaging of fixed cells was done using a LSM 880 confocal microscope (Zeiss) with a 63X oil objective. Analysis was performed using Imaris 9.6 (Oxford instruments). Live cell imaging was performed using a 3i Spinning Disc confocal microscope (Zeiss). Stag1-mNG-V5-FKBP12^{F36V} cells were seeded in an 8-chambered coverglass (Lab-Tek II) and DMSO or dTAG (500nM) were added for 24hr before imaging. Directly prior to imaging, cells were incubated with Hoechst 33342 (BD Pharmingen) for 45min, and then replaced with fresh 2i ESC media. Cells were imaged as confocal Z-stacks using DAPI and GFP lasers with a 63X objective and 1.4 Numerical Aperture.

Antibodies used in this study

Protein	Catalogue No.	Company	Figure references
Stag1/SA1, N-term epitope	ab4455	Abcam	1B, C, I, S1C, K, 2C, S2C, E, 3J, S3G, 4C, F, 5J
Stag1/SA1, C-term epitope	ab4457	Abcam	2F, S5A, 3I
Stag2/SA2	A300-158A	Bethyl	1B, S1C
Smc3	ab9263	Abcam	1B, 2C
Nanog	ab70482	Abcam	1E, S1F
Tubulin (Tub)	T5168	Sigma	1C, 1I, S2E, 4C, S6A
Actin	Mab8929	Novus	S1C
H3	ab1791	Abcam	1C
v5	14-6796-82	Invitrogen	3K
HP1a	2616	Cell Signalling	2C, S2B, C
Nucleolin (Ncl)	ab22758	Abcam	2C, 5J, 6A, S6A
POLR2	MMS-128P	Covance	3K, L
H3K9me3	ab8898	Abcam	2F, I, S2E, 5A, S5A
H3K4me3	ab8580	Abcam	S2E
Alexa488-anti-GFP (GFP)	A-21311	ThermoFisher	2I, S2A, B, 5A
Trim28	MA1-2023	ThermoFisher	5J

825 **Nascent transcription and translation analysis**

826 For nascent transcription analysis, we used the Click-iT® RNA Alexa Fluor® 488 HCS Assay
827 (Invitrogen C10327). ES cells were labelled with 1mM EU for 45min at 37C in fresh ES
828 media. Cells were fixed in solution or onto coverslips with 3.7% paraformaldehyde and
829 permeabilised with 0.5% Triton-X solution. Cells were incubated with the Click-iT
830 reaction cocktail for 30min. Cells were then either processed further for
831 Immunofluorescence as per methods described above (directly to the blocking step) or
832 analysed by flow cytometry on a BD Fortessa X20. For the Nascent translation analysis,
833 Click-iT™ HPG Alexa Fluor™ 594 Protein Synthesis Assay Kit (Invitrogen C10429) was used.
834 Cells were pre-incubated in Methionine-free media for 30 min in the 37C incubator before
835 addition of L-homopropargylglycine (HPG) at 50μM. Cells were incubated with HPG for 30 min,
836 then collected, fixed, permeabilized, and stained using Click-It reaction in low retention tubes.
837 HPG incorporation was measured by Flow Cytometry. FACS analysis (in Figures 5,6) was done
838 with FloJo software (version 10.7.1).

839

840 **Next generation Sequencing and Analysis**

841 Genomic data generated in this study (RNA-seq, PacBio-seq and UMI4C-seq) was submitted to
842 GEO with the Accession GSE160390.

843 **RNA sequencing (RNA-seq) library preparation and sequencing**

844 ESCs were treated for 24hrs with siRNA pools to Stag1 (SA1) and two sets of control siRNAs,
845 scrambled (SCR) and Luciferase (Luc). There are three replicate sets for SP KD and two for the
846 siRNA pools (SATS, 3p, 5p). Total RNA was isolated using NEB Monarch RNA prep kit. 1μg of
847 total RNA was rRNA-depleted using NEBNext rRNA depletion kit (Human/Mouse/Rat). Libraries
848 were prepared from 10-50ng rRNA-depleted total RNA, depending on availability of material,
849 using NEBNext Ultra II directional RNAseq kit according to manufacturer's instructions using 8
850 cycles of PCR. All ESC FCS libraries were rRNA depleted and only the ESC 2i libraries were
851 PolyA-enriched before library prep. Two rounds of PolyA+ enrichment were performed. RNA-
852 seq libraries were sequenced on the Illumina HiSeq3000 platform, 75bp paired-end or single-
853 end reads. Reads were quality controlled using FASTQC. RNA-seq data was processed using
854 the RNA-seq Nextflow pipeline (v19.01.0), with the following parameters –aligner hisat2 –
855 genome mm10, with –reverse_stranded specified for paired-end samples. FeatureCounts
856 output was parsed through edgeR (v3.16.5) and DESeq2 (v1.14.1) to generate normalised
857 expression counts. The normalised counts for RNAseq (Figure 1) were calculated in edgeR.

858 Low expressed genes were removed (rowSum cpm <2 across SCR and SA1SP replicates),
859 normalisation factors were calculated using calcNormFactors and dispersions estimated using
860 estimateDisp. The edgeR volcano plot statistics were calculated using the exactTest and
861 topTags functions. To generate the normalised counts for RNAseq experiments required to
862 calculate the log2FC GSEA ranked lists, the FeatureCounts output for all experiments was
863 combined into a single table and read into DESeq2. A DESeq2 object was built using the
864 function DESeqDataSetFromMatrix and estimation of size factors and dispersions were
865 calculated using the DEseq function. Normalised counts were calculated using the 'counts'
866 function. Low expressed genes (rowSum normalised count <10 across all samples) were
867 removed.
868
869 **GSEA**
870 Broad Institute GSEAPreranked (v4.0.3) was used to determine the enrichment of curated
871 genesets within our RNA-seq data. For each sample a ranked list was generated with genes
872 ranked in descending order by their log2FC value using normalised expression scores from
873 DEseq2. Log2FC per gene was calculated between the KD and its respective SCR using the
874 following calculation: Log2(normalised_counts KD +1) - log2(normalised_counts SCR +1). In
875 the case of experiments with multiple KD replicates, the average log2 normalised count was
876 used. Three gene sets were assayed in this study, 'naïve pluripotency', 'primed pluripotency'
877 and '2C signatures'. The naïve and primed pluripotency gene sets were curated in-house from
878 Fidalgo M et al. (CSC, 2016) where genes were selected if they had ≥2 fold change. The naïve
879 and primed gene sets contained 661 and 580 genes respectively. The 2C signatures gene set
880 (147 genes) was obtained from Percharde M et al. (Cell, 2018). Gene sets were classed as
881 having significant enrichment if the p-value was ≤0.05 and the normalised enrichment score
882 (NES) exceeded +/- 1.
883
884 **VAST-TOOLS**
885 VAST-TOOLS was used to generate Percent Spliced In (PSI) scores, a statistic which
886 represents how often a particular exon is spliced into a transcript using the ratio between reads
887 which include and exclude said exon. Paired-end RNA-seq datasets were submitted to VAST-
888 TOOLS (v2.1.3) using the Mmu genome (Tapial J et al, Gen Res 2017). Briefly, reads are split
889 into 50nt words with a 25nt sliding window. The 50nt words are aligned to a reference genome
890 using Bowtie to obtain unmapped reads. These unmapped reads are then aligned to a set of

891 predefined exon-exon junction (EJJ) libraries allowing for the quantification of alternative exon
892 events. The output was further interrogated using a script which searches all hypothetical EEJ
893 combinations between potential donors and acceptors within Stag1. PSI scores could be
894 obtained providing there was at least a single read within our RNAseq data that supported one
895 of these potential events. Some datasets were combined to have enough reads for the analysis.
896 See Table S1 for PSI values and names of RNA-seq libraries used for analysis in Fig. 3e, S4b.
897
898 **Quantifying sectioned Stag1**
899 Stag1 was split into 5 sections; SATS, e1-e8, e12-e19, e20-e25, e26-e34. Using Kallisto
900 (v0.46.1), raw RNAseq reads were used to quantify each section of Stag1. Kallisto was run in
901 quant mode, using the –rf-stranded parameter, outputting a TPM per Stag1 section. A line plot
902 was generated showing TPM in relative to UT.
903
904 **PacBio library, sequencing and analysis**
905 ES cells were cultured in naïve 2i conditions and PolyA-enriched mRNAs were hybridized to a
906 custom Biotinylated oligonucleoltide probe set. Post-capture, mRNAs were amplified using the
907 Clontech SMARTer PCR cDNA Synthesis Kit with 9 cycles and used in the SMRTbell library
908 prep according to manufacturers instructions. The library was sequenced on the SMRTseq 2000
909 platform. PacBio reads were processed through the SMRTLINK v8.0.0 IsoSeq3 pipeline.
910 403,995 Circular consensus sequences (CCS) were generated using default parameters (--
911 minPasses = 1, --min-rq = 0.8, CCS Polish = No). Further refining through lima (removal of
912 adapters and correct orientation of sequences), poly-A trimming and concatemer removal
913 resulted in 265,106 full length non-chimeric (FLNC) reads. FLNC reads were aligned to the
914 mm10 genome using Minimap2 with the following parameters (-ax splice, -uf, -k14).
915
916 **ChIP-seq Analysis**
917 Previously published Stag1 Chromatin Immunoprecipitation-sequencing (ChIP-seq) datasets
918 from ES 2i cells (GSE126659, only Replicate 1 and 2 libraries) were trimmed using trim_galore
919 and aligned to mm10 using bowtie2. Peak detection was performed with MACS2 using uniquely
920 reads (MAPQ≥2). Peaks were overlapped with genomic features in a hierarchical manner
921 (promoters > exons > repeats > introns > intergenic), and overlap frequency was compared with
922 a randomly shuffled version of the peaks. To identify repeat families enriched for STAG1 peaks,
923 a previously described pipeline was used (Deniz O et al. Nat Comm, 2020) that compares

924 family-levels overlap frequency with that observed in 1,000 permutations of random peak
925 shuffling. Coverage profiles across specific TE families were generated using HOMER and
926 including multi-mapping reads (MAPQ<2).
927
928 **UMI-4C library preparation.**
929 1x10^7 cells were fixed at RT for 10min in 1% formaldehyde and fixation was quenched with
930 0.125M Glycine for 5min. Cells were then lysed on ice in 10ml Lysis Buffer (10mM NaCl, 10mM
931 Tris-HCl pH 8.0, 0.25% NP40, protease inhibitor) for 30min, followed by 10 strokes of douncing
932 using a tight pestle. Nuclei were pelleted, 8min 700 rcf, washed in 1ml 1.2X DpnII buffer in
933 Protein LoBind tubes (Eppendorf) and resuspended in 500 μl 1.2X DpnII buffer. 15ul of 10%
934 SDS was added and incubated for 1hr at 37°C shaking at 650 rcf. 50ul of 20% TritonX was
935 added to quench the SDS and incubated for 15 min at 37°C with shaking. 750U of DpnII was
936 added and incubated overnight at 37**°C** with interval shaking. The next morning, nuclei were
937 pelleted at 4°C by 650 rcf for 5 min and resuspended in 500μl 1X DpnII buffer. 500U DpnII was
938 added and incubated for an additional four hours. The nuclei were washed twice in 100 μl of 1X
939 T4 Ligase Buffer and resuspended in 200 μl Ligase Buffer. 6ul of T4 DNA Ligase was added
940 and incubated for 3hr at 16°C**.** Nuclei were then pelleted, resuspended in 200 μl 1x fresh Ligase
941 Buffer, 6μl of T4 DNA Ligase added, and incubated overnight at 16°C. Samples were treated
942 with 20μl of ProtK (NEB Molecular Biology Grade), incubated for 3 hrs at 55°C and 5 hrs at
943 65°C to reverse crosslinks. Samples were treated with RNase A (PureLink, Invitrogen) for 1 hr
944 at 37°C and DNA was extracted and precipitated overnight. For library preparation, 3x5μg of
945 ligated DNA was sonicated using Covaris (10% duty cycle, intensity 5, cycle burst 200, 70sec).
946 Samples were end-repaired using DNA PolII Klenow Large Fragment (NEB), A-tailed using
947 Klenow (exo-) (NEB), and Illumina indexed adapters ligated using Quick DNA Ligase (NEB).
948 Reactions were denatured at 95°C for 3 min, placed on ice, and purified using 1.2X SizeSelect
949 AmpPure beads to recover ssDNA. Libraries were amplified using GoTaq (Promega), with 20
950 cycles for PCR1 and 15 cycles for nested PCR2 on 50% material from 1st PCR. For custom UMI
951 bait sequences, see Table S3.
952
953 **Hi-C and UMI-4C-seq analysis**
954 Hi-C libraries were analysed as previously described (Barrington 2019). UMI-4C tracks were
955 processed using the 'umi4cPackage' pipeline (v0.0.0.9000) (Schwartzman, O et al. Nat Meth

956 2017). Briefly, raw reads are parsed through the UMI-4C pipeline, those reads containing the
957 bait and padding sequence are retained and de-multiplexed. Reads lacking the padding
958 sequence are considered non-specific and are removed from further analysis. Retained reads
959 are split based on a match to the restriction enzyme sequence to create a segmented fastq file.
960 The first 10 bases of read 2 are extracted and attached to the segments derived from each read
961 pair. Mapping to mm10 is done with Bowtie2. Read pairs that have reverse complement
962 segments are mapped to a restriction fragment ID, with the fragment ID, strand and distance
963 from each end represented within a fragment-chain table. UMI filtering is used to determine the
964 number of molecules supporting each ligation event. The resulting UMI-4C tracks are then
965 imported into R, and data from multiple bait replicates can be merged by summing the molecule
966 counts per ligated fragment, at which point contact intensity profiles and domainograms around
967 the viewpoint can be generated (see Figure 3). The contact intensity profile represents the
968 mean number of ligations within a genomic window, with the resolution of the contact intensity
969 profile being determined by the window size (set to 15 here). The domainogram reports the
970 mean contact per fend at a series of window sizes, a stacked representation of contact intensity
971 values in increasing window sizes from 10 to 300 fragment ends, their colour can be used to
972 identify peak locations. ES and NSC contact profiles were compared after normalisation to
973 correct for bias (see Schwartzman et al for further details). For the compared profiles, the total
974 molecule count for restriction fragment ends for each are calculated at three ranges around the
975 viewpoint. One profile is selected as a reference and the second is scaled to the first using the
976 ratio in total molecule counts between the two profiles as the scaling factor. Below the contact
977 profile is the profile resolution indicator, which shows the number of fends required to include at
978 least 15 UMI molecules. The darker the colour, the larger the window size required. The
979 domainogram at the bottom represents the log2 ratio between the domainogram values of the
980 compared profiles and highlights locations where ESC has more contacts than NSC or vice
981 versa.

982 **REFERENCES**

983 1. Horsfield, J. A. *et al.* Cohesin-dependent regulation of Runx genes. *Development*
984 **134,** 2639–2649 (2007).
985 2. Viny, A. D. *et al.* Cohesin Members Stag1 and Stag2 Display Distinct Roles in
986 Chromatin Accessibility and Topological Control of HSC Self-Renewal and
987 Differentiation. *Cell Stem Cell* **25,** 682–696.e8 (2019).
988 3. Leiserson, M. D. M. *et al.* Pan-cancer network analysis identifies combinations of
989 rare somatic mutations across pathways and protein complexes. *Nat. Genet.* **47,**
990 106–114 (2015).
991 4. Romero-Pérez, L., Surdez, D., Brunet, E., Delattre, O. & Grünewald, T. G. P. STAG
992 Mutations in Cancer. *Trends Cancer* **5,** 506–520 (2019).
993 5. Cuartero, S. *et al.* Control of inducible gene expression links cohesin to
994 hematopoietic progenitor self-renewal and differentiation. *Nat Immunol* **19,** 932–941
995 (2018).
996 6. Kline, A. D. *et al.* Diagnosis and management of Cornelia de Lange syndrome: first
997 international consensus statement. *Nat. Rev. Genet.* **19,** 649–666 (2018).
998 7. Hadjur, S. *et al.* Cohesins form chromosomal cis-interactions at the
999 developmentally regulated IFNG locus. *Nature* **460,** 410–413 (2009).
1000 8. Phillips-Cremins, J. E. *et al.* Architectural protein subclasses shape 3D organization
1001 of genomes during lineage commitment. *Cell* **153,** 1281–1295 (2013).
1002 9. Wendt, K. S. *et al.* Cohesin mediates transcriptional insulation by CCCTC-binding
1003 factor. *Nature* **451,** 796–801 (2008).
1004 10. Parelho, V. *et al.* Cohesins functionally associate with CTCF on mammalian
1005 chromosome arms. *Cell* **132,** 422–433 (2008).
1006 11. Mishiro, T. & Tsutsumi, S. Architectural roles of multiple chromatin insulators at the
1007 human apolipoprotein gene cluster. *EMBO J.* **28,** 1234–1245 (2009).
1008 12. Kagey, M. H. *et al.* Mediator and cohesin connect gene expression and chromatin
1009 architecture. *Nature* **467,** 430–435 (2010).
1010 13. Misulovin, Z. *et al.* Association of cohesin and Nipped-B with transcriptionally active
1011 regions of the Drosophila melanogaster genome. *Chromosoma* **117,** 89–102
1012 (2007).
1013 14. Vietri Rudan, M. *et al.* Comparative Hi-C reveals that CTCF underlies evolution of
1014 chromosomal domain architecture. *CellReports* **10,** 1297–1309 (2015).
1015 15. Rao, S. S. P. *et al.* A 3D map of the human genome at kilobase resolution reveals
1016 principles of chromatin looping. *Cell* **159,** 1665–1680 (2014).
1017 16. Sofueva, S. *et al.* Cohesin-mediated interactions organize chromosomal domain
1018 architecture. *EMBO J.* **32,** 3119–3129 (2013).
1019 17. Zuin, J. *et al.* Cohesin and CTCF differentially affect chromatin architecture and
1020 gene expression in human cells. *Proc. Natl. Acad. Sci. U.S.A.* **111,** 996–1001
1021 (2014).
1022 18. Rao, S. S. P. *et al.* Cohesin Loss Eliminates All Loop Domains. *Cell* **171,** 305–
1023 309.e24 (2017).
1024 19. Seitan, V. C. *et al.* Cohesin-based chromatin interactions enable regulated gene
1025 expression within preexisting architectural compartments. *Genome Res.* **23,** 2066–
1026 2077 (2013).
1027 20. Schwarzer, W. *et al.* Two independent modes of chromatin organization revealed
1028 by cohesin removal. *Nature* **551,** 51–56 (2017).
1029 21. Wutz, G. *et al.* Topologically associating domains and chromatin loops depend on

1030 cohesin and are regulated by CTCF, WAPL, and PDS5 proteins. *EMBO J.* **36,**
1031 3573–3599 (2017).
1032 22. Haarhuis, J. H. I. *et al.* The Cohesin Release Factor WAPL Restricts Chromatin
1033 Loop Extension. *Cell* **169,** 693–707.e14 (2017).
1034 23. Lehalle, D. *et al.* STAG1 mutations cause a novel cohesinopathy characterised by
1035 unspecific syndromic intellectual disability. *J Med Genet* **54,** 479–488 (2017).
1036 24. Soardi, F. C. *et al.* Familial STAG2 germline mutation defines a new human
1037 cohesinopathy. *NPJ Genom Med* **2,** 7–11 (2017).
1038 25. Yuan, B. *et al.* Clinical exome sequencing reveals locus heterogeneity and
1039 phenotypic variability of cohesinopathies. *Genet Med* **21,** 663–675 (2019).
1040 26. Cuadrado, A. *et al.* Specific Contributions of Cohesin-SA1 and Cohesin-SA2 to
1041 TADs and Polycomb Domains in Embryonic Stem Cells. *Cell Rep* **27,** 3500–
1042 3510.e4 (2019).
1043 27. Hara, K. *et al.* Structure of cohesin subcomplex pinpoints direct shugoshin-Wapl
1044 antagonism in centromeric cohesion. *Nature Publishing Group* **21,** 864–870 (2014).
1045 28. Xiao, T., Wallace, J. & Felsenfeld, G. Specific sites in the C terminus of CTCF
1046 interact with the SA2 subunit of the cohesin complex and are required for cohesin-
1047 dependent insulation activity. *Mol. Cell. Biol.* **31,** 2174–2183 (2011).
1048 29. Li, Y. *et al.* The structural basis for cohesin-CTCF-anchored loops. *Nature* **578,**
1049 472–476 (2020).
1050 30. Orgil, O. *et al.* A conserved domain in the scc3 subunit of cohesin mediates the
1051 interaction with both mcd1 and the cohesin loader complex. *PLoS Genet.* **11,**
1052 e1005036 (2015).
1053 31. Canudas, S. & Smith, S. Differential regulation of telomere and centromere
1054 cohesion by the Scc3 homologues SA1 and SA2, respectively, in human cells. *J*
1055 *Cell Biol* **187,** 165–173 (2009).
1056 32. Kojic, A. *et al.* Distinct roles of cohesin-SA1 and cohesin-SA2 in 3D chromosome
1057 organization. *Nature Publishing Group* **25,** 496–504 (2018).
1058 33. Remeseiro, S. *et al.* Cohesin-SA1 deficiency drives aneuploidy and tumourigenesis
1059 in mice due to impaired replication of telomeres. *EMBO J.* **31,** 2076–2089 (2012).
1060 34. Winters, T., McNicoll, F. & Jessberger, R. Meiotic cohesin STAG3 is required for
1061 chromosome axis formation and sister chromatid cohesion. *EMBO J.* **33,** 1256–
1062 1270 (2014).
1063 35. Bisht, K. K., Daniloski, Z. & Smith, S. SA1 binds directly to DNA through its unique
1064 AT-hook to promote sister chromatid cohesion at telomeres. *J. Cell. Sci.* **126,** 3493–
1065 3503 (2013).
1066 36. Boisvert, F.-M., van Koningsbruggen, S., Navascués, J. & Lamond, A. I. The
1067 multifunctional nucleolus. *Nat. Rev. Mol. Cell Biol.* **8,** 574–585 (2007).
1068 37. Feric, M. *et al.* Coexisting Liquid Phases Underlie Nucleolar Subcompartments. *Cell*
1069 **165,** 1686–1697 (2016).
1070 38. Yao, R.-W. *et al.* Nascent Pre-rRNA Sorting via Phase Separation Drives the
1071 Assembly of Dense Fibrillar Components in the Human Nucleolus. *Molecular Cell*
1072 **76,** 767–783.e11 (2019).
1073 39. Padeken, J. & Heun, P. Nucleolus and nuclear periphery: velcro for
1074 heterochromatin. *Curr. Opin. Cell Biol.* **28,** 54–60 (2014).
1075 40. Kresoja-Rakic, J. & Santoro, R. Nucleolus and rRNA Gene Chromatin in Early
1076 Embryo Development. *Trends Genet.* **35,** 868–879 (2019).
1077 41. Aguirre-Lavin, T. *et al.* 3D-FISH analysis of embryonic nuclei in mouse highlights
1078 several abrupt changes of nuclear organization during preimplantation

development. *BMC Dev Biol* **12,** 30–20 (2012).
42. Fulka, H., Rychtarova, J. & Loi, P. The nucleolus-like and precursor bodies of mammalian oocytes and embryos and their possible role in post-fertilization centromere remodelling. *Biochemical Society Transactions* **48,** 581–593 (2020).
43. Ishiuchi, T. *et al.* Early embryonic-like cells are induced by downregulating replication-dependent chromatin assembly. *Nature Publishing Group* **22,** 662–671 (2015).
44. Xie, S. Q. *et al.* Nucleolar-based Dux repression is essential for embryonic two-cell stage exit. *Genes Dev.* **36,** 331–347 (2022).
45. Németh, A. *et al.* Initial genomics of the human nucleolus. *PLoS Genet.* **6,** e1000889 (2010).
46. Gupta, S. & Santoro, R. Regulation and Roles of the Nucleolus in Embryonic Stem Cells: From Ribosome Biogenesis to Genome Organization. *Stem Cell Reports* **15,** 1206–1219 (2020).
47. Grow, E. J. *et al.* p53 convergently activates Dux/DUX4 in embryonic stem cells and in facioscapulohumeral muscular dystrophy cell models. *Nat. Genet.* **53,** 1207–1220 (2021).
48. Sun, Z. *et al.* LIN28 coordinately promotes nucleolar/ribosomal functions and represses the 2C-like transcriptional program in pluripotent stem cells. *Protein Cell* 1–23 (2021). doi:10.1007/s13238-021-00864-5
49. Laloraya, S., Guacci, V. & Koshland, D. Chromosomal addresses of the cohesin component Mcd1p. *Journal of Cell Biology* **151,** 1047–1056 (2000).
50. Harris, B. *et al.* Cohesion promotes nucleolar structure and function. *Mol Biol Cell* **25,** 337–346 (2014).
51. Mootha, V. K. *et al.* PGC-1alpha-responsive genes involved in oxidative phosphorylation are coordinately downregulated in human diabetes. *Nat. Genet.* **34,** 267–273 (2003).
52. Subramanian, A. *et al.* Gene set enrichment analysis: a knowledge-based approach for interpreting genome-wide expression profiles. *Proc Natl Acad Sci USA* **102,** 15545–15550 (2005).
53. Nabet, B. *et al.* The dTAG system for immediate and target- specific protein degradation. *Nature Chemical Biology* **14,** 1–16 (2018).
54. Quinodoz, S. A. *et al.* Higher-Order Inter-chromosomal Hubs Shape 3D Genome Organization in the Nucleus. *Cell* **174,** 744–757.e24 (2018).
55. Deniz, Ö. *et al.* Endogenous retroviruses are a source of enhancers with oncogenic potential in acute myeloid leukaemia. *Nature Communications* **11,** 3506–14 (2020).
56. Percharde, M. *et al.* A LINE1-Nucleolin Partnership Regulates Early Development and ESC Identity. *Cell* **174,** 391–405.e19 (2018).
57. Hackett, J. A., Kobayashi, T., Dietmann, S. & Surani, M. A. Activation of Lineage Regulators and Transposable Elements across a Pluripotent Spectrum. *Stem Cell Reports* **8,** 1645–1658 (2017).
58. Dixon, J. R. *et al.* Topological domains in mammalian genomes identified by analysis of chromatin interactions. *Nature* **485,** 376–380 (2012).
59. Schwalie, P. C. *et al.* Co-binding by YY1 identifies the transcriptionally active, highly conserved set of CTCF-bound regions in primate genomes. *Genome Biol.* **14,** R148–15 (2013).
60. Rowe, H. M. *et al.* KAP1 controls endogenous retroviruses in embryonic stem cells. *Nature* **463,** 237–240 (2010).
61. Meshorer, E. *et al.* Hyperdynamic plasticity of chromatin proteins in pluripotent

1128 embryonic stem cells. *Dev. Cell* **10,** 105–116 (2006).
1129 62. Feng, G. *et al.* Ubiquitously expressed genes participate in cell-specific functions
1130 via alternative promoter usage. *EMBO Rep.* **17,** 1304–1313 (2016).
1131 63. Tapial, J. *et al.* An atlas of alternative splicing profiles and functional associations
1132 reveals new regulatory programs and genes that simultaneously express multiple
1133 major isoforms. *Genome Res.* **27,** 1759–1768 (2017).
1134 64. Barrington, C., Georgopoulou, D., Nature, D. P.2019. Enhancer accessibility and
1135 CTCF occupancy underlie asymmetric TAD architecture and cell type specific
1136 genome topology. *nature.com* doi:10.1038/s41467-019-10725-9
1137 65. Hendrickson, P. G. *et al.* Conserved roles of mouse DUX and human DUX4 in
1138 activating cleavage-stage genes and MERVL/HERVL retrotransposons. *Nat. Genet.*
1139 **49,** 925–934 (2017).
1140 66. Macfarlan, T. S. *et al.* Embryonic stem cell potency fluctuates with endogenous
1141 retrovirus activity. *Nature* **487,** 57–63 (2012).
1142 67. Eckersley-Maslin, M. A. *et al.* MERVL/Zscan4 Network Activation Results in
1143 Transient Genome-wide DNA Demethylation of mESCs. *Cell Rep* **17,** 179–192
1144 (2016).
1145 68. Remeseiro, S., Cuadrado, A., López, G. G., Pisano, D. G. & Losada, A. A unique
1146 role of cohesin-SA1 in gene regulation and development. *EMBO J.* **31,** 2090–2102
1147 (2012).
1148 69. Borsos, M. & Torres-Padilla, M.-E. Building up the nucleus: nuclear organization in
1149 the establishment of totipotency and pluripotency during mammalian development.
1150 *Genes Dev.* **30,** 611–621 (2016).
1151

Figure 1. *Pezic et al.*

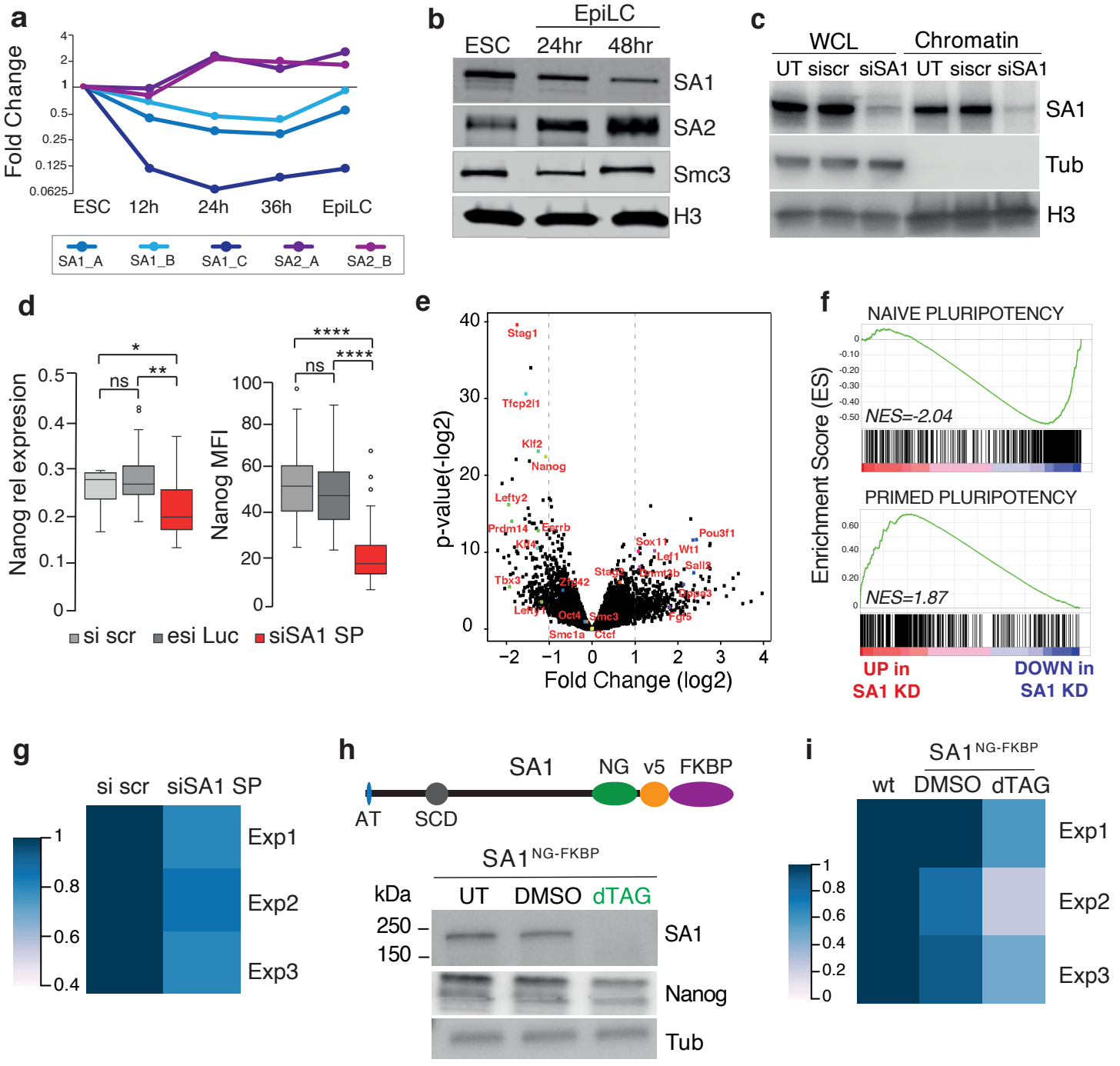

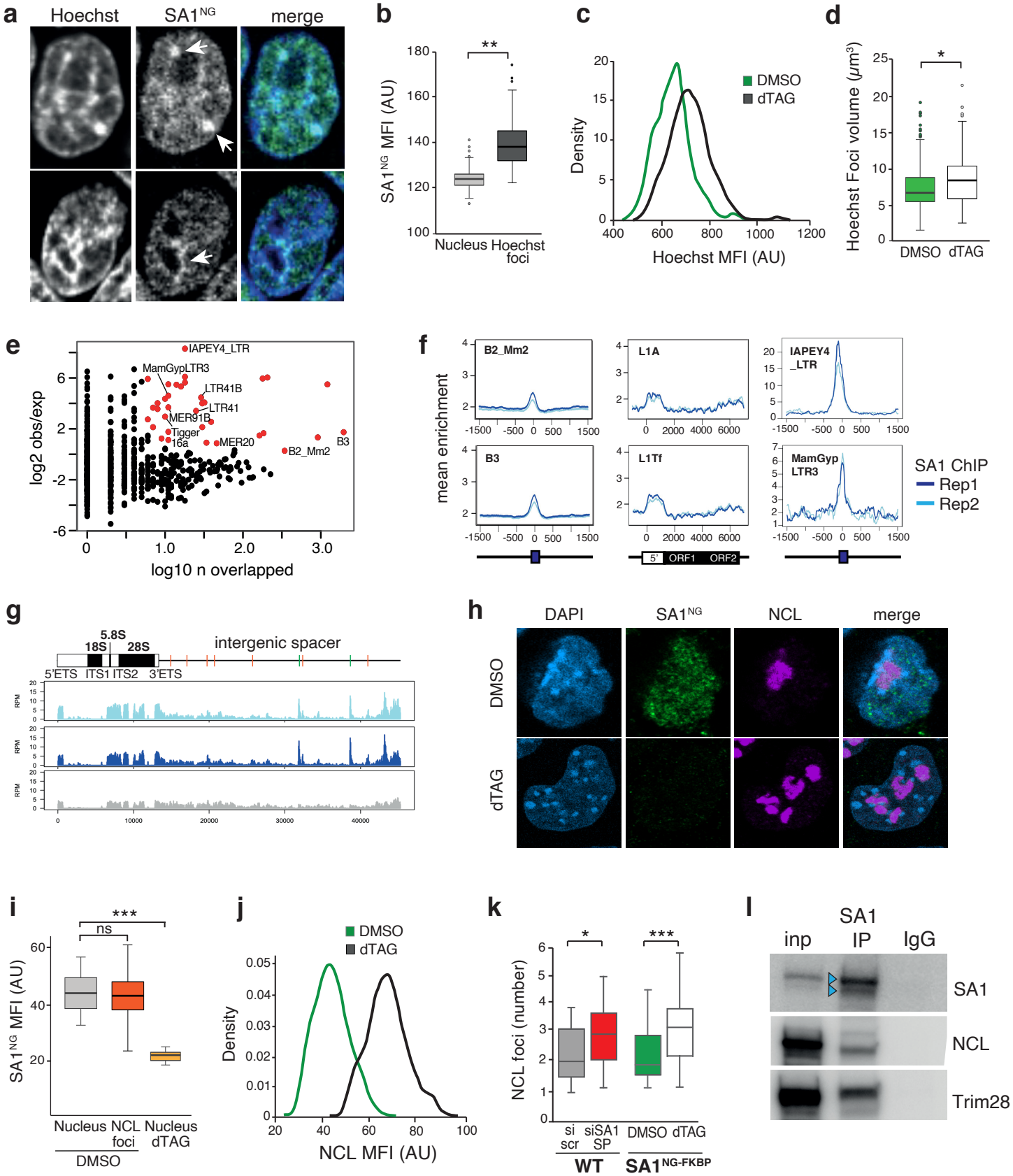
a
Hoechst
SA1NG
merge
b
SA1NG MFI (AU)
Nucleus
Hoechst foci
c
Density
DMSO
dTAG
Hoechst MFI (AU)
d
Hoechst Foci volume (μm3)
DMSO
dTAG
e
log2 obs/exp
log10 n overlapped
IAPEY4_LTR
MamGypLTR3
LTR41B
LTR41
MER91B
Tigger 16a
MER20
B2_Mm2
B3
f
mean enrichment
B2_Mm2
L1A
IAPEY4 _LTR
B3
L1Tf
MamGyp LTR3
5'
ORF1
ORF2
SA1 ChIP
Rep1
Rep2
g
5.8S
18S
28S
intergenic spacer
5'ETS
ITS1
ITS2
3'ETS
RPM
h
DAPI
SA1NG
NCL
merge
DMSO
dTAG
i
SA1NG MFI (AU)
ns
Nucleus
NCL foci
Nucleus dTAG
DMSO
j
DMSO
dTAG
Density
NCL MFI (AU)
k
NCL foci (number)
si scr
siSA1 SP
DMSO
dTAG
WT
SA1NG-FKBP
l
SA1
inp
IP
IgG
SA1
NCL
Trim28

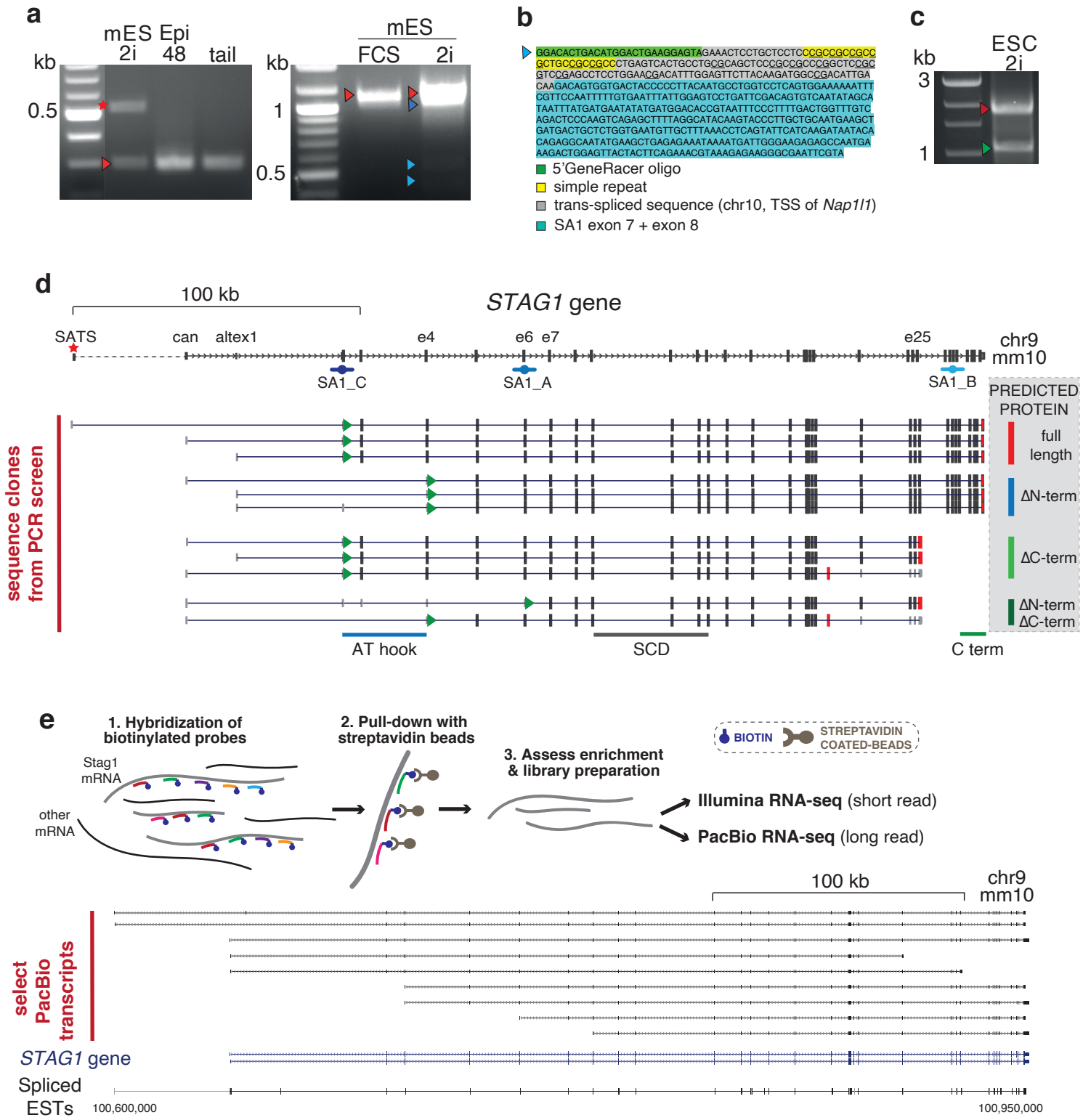
a
mES Epi
2i 48 tail
kb
0.5
mES
FCS 2i
kb
1
0.5
b
GGACACTGACATGGACTGAAGGAGTAGAAACTCCTGCTCCTCCCGCCGCCGCC
GCTGCCGCCGCCCCTGAGTCACTGCCTGCGCAGCTCCCGCCGCCCGGCTCCGC
GTCCGAGCCTCCTGGAACGACATTTGGAGTTCTTACAAGATGGCCGACATTGA
CAAGACAGTGGTGACTACCCCCTTACAATGCCTGGTCCTCAGTGGAAAAAATTT
CGTTCCAATTTTTGTGAATTTATTGGAGTCCTGATTCGACAGTGTCAATATAGCA
TAATTTATGATGAATATATGATGGACACCGTAATTTCCCTTTTGACTGGTTTGTC
AGACTCCCAAGTCAGAGCTTTTAGGCATACAAGTACCCTTGCTGCAATGAAGCT
GATGACTGCTCTGGTGAATGTTGCTTTAAACCTCAGTATTCATCAAGATAATACA
CAGAGGCAATATGAAGCTGAGAGAAATAAAATGATTGGGAAGAGAGCCAATGA
AAGACTGGAGTTACTACTTCAGAAACGTAAAGAGAAGGGCGAATTCGTA
5'GeneRacer oligo
simple repeat
trans-spliced sequence (chr10, TSS of Nap1l1)
SA1 exon 7 + exon 8
c
ESC
2i
kb
3
1
d
100 kb
STAG1 gene
SATS
can
altex1
e4
e6 e7
e25
chr9
mm10
SA1_C
SA1_A
SA1_B
PREDICTED PROTEIN
full length
ΔN-term
ΔC-term
ΔN-term ΔC-term
sequence clones from PCR screen
AT hook
SCD
C term
e
1. Hybridization of biotinylated probes
2. Pull-down with streptavidin beads
3. Assess enrichment & library preparation
BIOTIN
STREPTAVIDIN COATED-BEADS
Stag1 mRNA
other mRNA
Illumina RNA-seq (short read)
PacBio RNA-seq (long read)
100 kb
chr9
mm10
select PacBio transcripts
STAG1 gene
Spliced ESTs
100,600,000
100,950,000
f
IP
kDa
inp
SA1
IgG
150
100
75
50
g
si scr
si SA1
kDa
150
100
75
H3
h
SA1NG-FKBP
+DMSO
+dTAG
V5 IP
kDa
inp
IgG
250
150
100
50

Figure 4. *Pezic et al.*

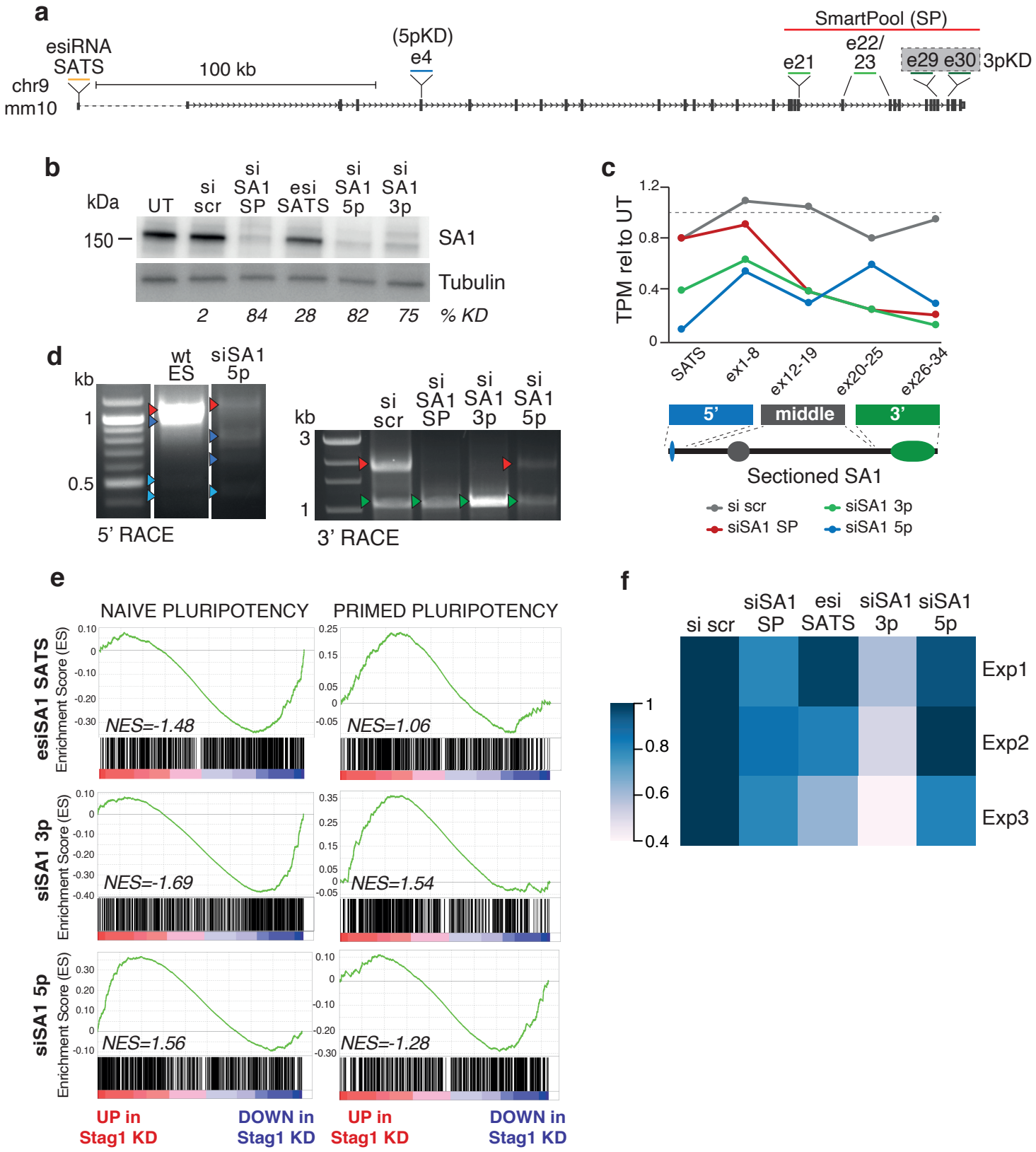

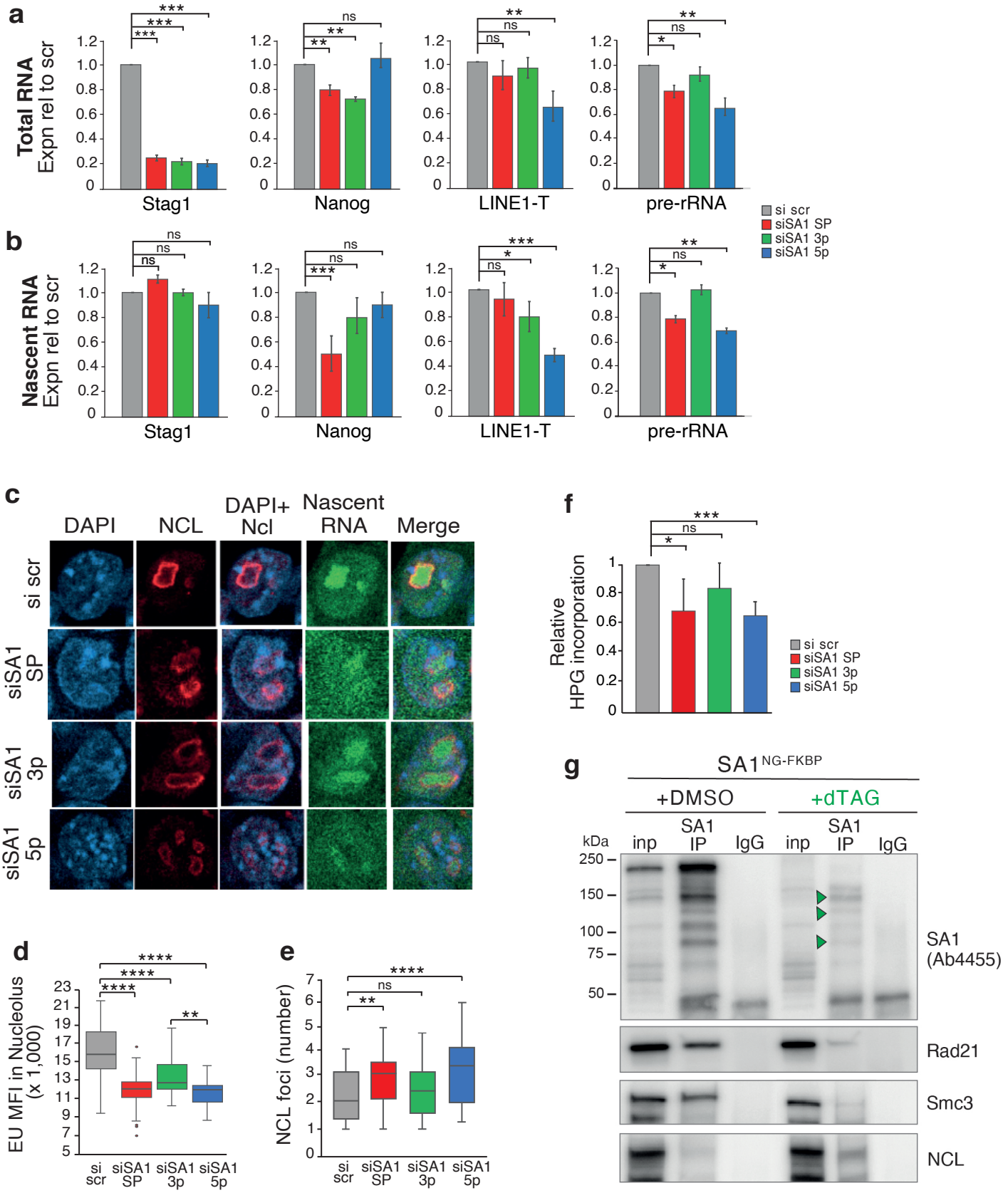
a
Total RNA
Expn rel to scr
Stag1
Nanog
LINE1-T
pre-rRNA
b
Nascent RNA
Expn rel to scr
si scr
siSA1 SP
siSA1 3p
siSA1 5p
c
DAPI
NCL
DAPI+ Ncl
Nascent RNA
Merge
d
EU MFI in Nucleolus (x 1,000)
e
NCL foci (number)
f
Relative HPG incorporation
g
SA1NG-FKBP
+DMSO
+dTAG
kDa
inp
SA1 IP
IgG
SA1 (Ab4455)
Rad21
Smc3
NCL

Figure 6.
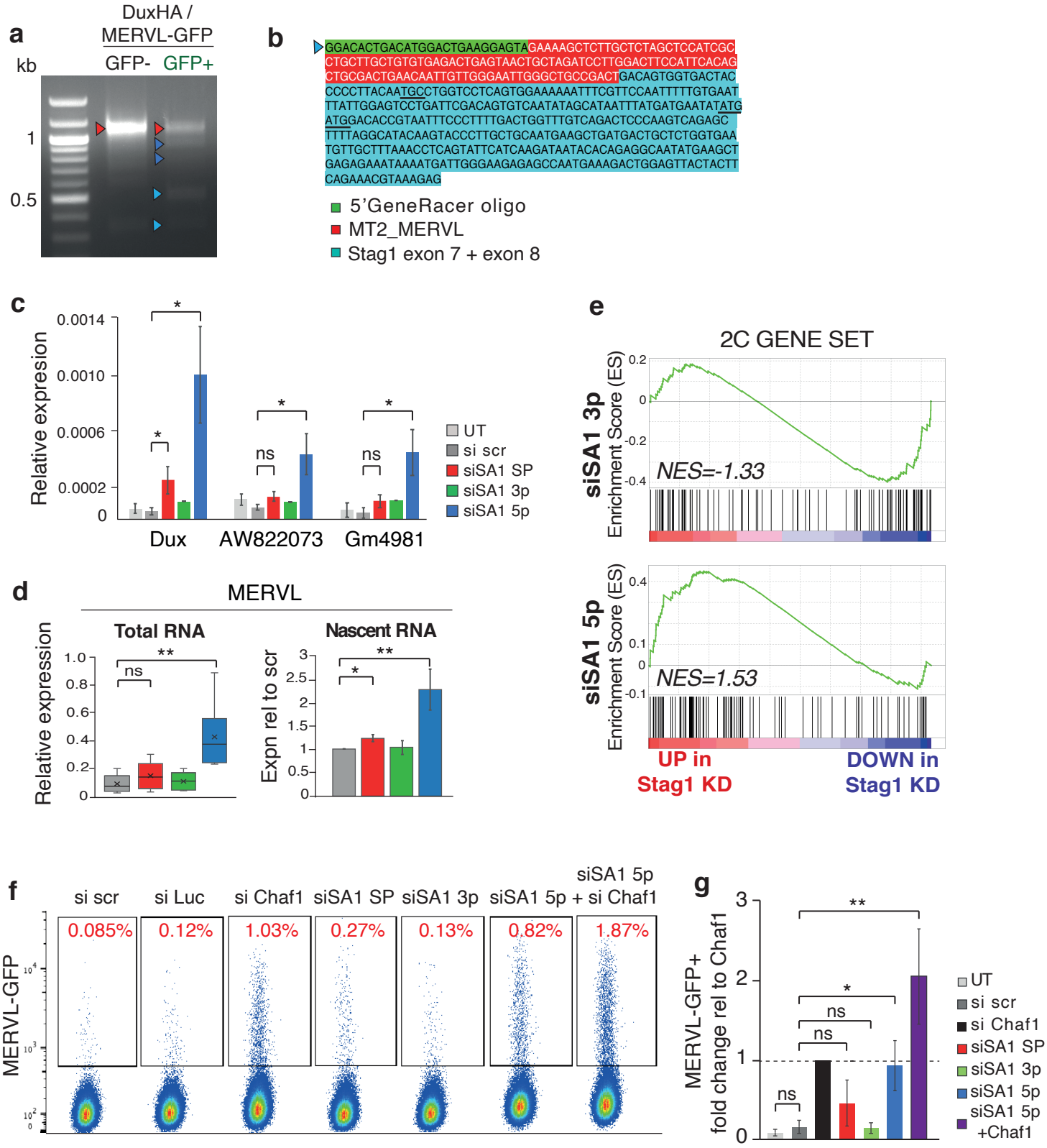
Pezic et al.